TECHNISCHE UNIVERSITÄT WIEN

Energy Economics Group

Master's Thesis

for the achievement of the academic degree

Diplom-Ingenieur

in the field of study Energy Systems and Automation Technology
at TU Wien

A quantitative analysis of the temporal and spatial distribution of charging flexibility of electrified trucks in Austria

submitted at
Institute of Energy Systems and Electrical Drives

Supervisor: Associate Prof. Dipl.-Ing. Dr.techn. Johann Auer
Assistent: Dipl-Ing. Dr.techn. Christoph Loschan

by

Nikolaus Heiner Diez, BSc
51835509

Wien, January 2025

Abstract

Increasing flexibility in the energy sector is a key factor for achieving a climate-friendly energy transition through the enhanced integration of renewable energy sources across Europe. In addition to better integrating renewable energies, demand-side flexibility in the energy sector, in particular, can be used to reduce costs and emissions, relieve the transmission and distribution grids, and reduce redispatch measures.
This thesis focuses on modeling and quantifying the flexibility potential of electrified trucks in Austria. The simulation of this potential is an essential step to understand better the possible interactions between the transport and energy sectors and to classify the potential spatially and temporally. This enables the development of scenarios in which electrified trucks function not only as a means of transportation but also as active participants in the energy market, as flexibility providers.
The bottom-up model developed in this study analyzes all truck fleets operating on routes impacting Austria to calculate the corresponding flexibility potential for specific times of day and regions. This modeling approach enables the first-ever estimation of the spatial distribution of flexibility from electrified truck traffic in Austria.
The results indicate that, on average, more than 400 *MW* of reserve power can be available as flexibility for a 15 *min* time interval throughout Austria by 2030. The Linz-Wels region, in particular, shows significant usable flexibility during the morning, late morning, and afternoon hours, extending into the early morning. However, little usable flexibility is available early in the morning when the night driving ban concludes and at lunchtime. A stark contrast exists between the northeastern regions, traversed by the A1, A21, and A8 freeways, which exhibit high reserve capacities, and the other regions of Austria, which generally have lower reserve power. Flexibility is highly sensitive to truck speed and the installed capacities.
Future research could analyze the local alignment between existing flexibility from battery-electric truck traffic and the necessary redispatch measures and extend the model for EU-wide forecasts.

Kurzfassung

Die Erhöhung der Flexibilität im Energiesektor stellt einen Schlüsselfaktor für eine klimafreundliche Energiewende durch die verstärkte Integration erneuerbarer Energien in Europa dar. Neben der besseren Integration erneuerbarer Energien kann insbesondere nachfrageseitige Flexibilität im Energiesektor zur Kosten- und Emissionsreduktion, zur Entlastung der Übertragungs- und Verteilnetze, sowie zur Reduktion von Redispatch-Maßnahmen eingesetzt werden.
Ziel dieser Arbeit ist die Modellierung und Quantifizierung des Flexibilitätspotentials elektrifizierter Lkw in Österreich. Die Simulation dieses Potentials ist ein wesentlicher Schritt, um die möglichen Wechselwirkungen zwischen Verkehrs- und Energiesektor besser zu verstehen und das Potential räumlich und zeitlich einordnen zu können. Dies ermöglicht die Entwicklung von Szenarien, in denen elektrifizierte Lkw nicht nur als Transportmittel, sondern auch als aktive Teilnehmer am Energiemarkt, als Flexibilitätsanbieter, fungieren.
Mit dem entwickelten Bottom-up-Modell erfolgt eine Simulation sämtlicher LKW-Flotten auf allen LKW-Routen, die Österreich betreffen. Ziel dieser Simulation ist die Berechnung des Flexibilitätspotenzials für spezifische Tageszeiten und Regionen. Der entwickelte Modellierungsansatz erlaubt erstmals eine Abschätzung der räumlichen Verteilung der Flexibilität des elektrifizierten LKW-Verkehrs in Österreich.
Die Ergebnisse zeigen, dass im Jahr 2030 österreichweit im Mittel über 400 *MW* für einen Zeitschritt von 15 *min* als Flexibilität zur Verfügung stehen können. Insbesondere die östliche Region Linz-Wels zeichnet sich durch nutzbare Flexibilität in den Morgen-, Vormittags- und Nachmittagsstunden bis in die frühen Morgenstunden aus. Lediglich frühmorgens, wenn das Nachtfahrverbot in Österreich endet, und in der Mittagszeit ist wenig nutzbare Flexibilität vorhanden. Es zeigt sich ein signifikantes Gefälle zwischen den nordöstlichen Regionen, welche von den Autobahnen A1, A21 und A8 durchquert werden, und den übrigen Regionen Österreichs. Erstere verfügen über hohe Reserveleistungen, während Letztere überwiegend geringe Reserveleistungen aufweisen. Es konnte eine hohe Sensitivität der Flexibilität gegenüber der gefahrenen Geschwindigkeit der LKW und der installierten Kapazitäten festgestellt werden.
Weitere Arbeiten könnten sich mit der Analyse der lokalen Übereinstimmung zwischen der vorhandenen Flexibilität des batterieelektrischen Lkw-Verkehrs und den erforderlichen Redispatch-Maßnahmen befassen. Zudem wäre eine Erweiterung des Modells für EU-weite Prognosen denkbar.

Contents

List of Figures

List of Tables

List of Acronyms

ASFINAG	Autobahnen- und Schnellstraßen-Finanzierungs-Aktiengesellschaft
BET	Battery electric truck
E-road	Freeways (”Autobahnen”) and national roads (”Bundesstraßen”) in Europe
EU	European Union
EV	Electric vehicle
HDV	Heavy-duty vehicle
NUTS	Nomenclature des Unités territoriales statistiques
PV	Photovoltaic
SoC	State of Charge
V2G	Vehicle-to-grid

1 Introduction

1.1 Motivation and Background

Climate change is one of the greatest challenges of our time. The European Union (EU) has set ambitious targets to shape a sustainable energy future and meet its climate commitments under the Paris Agreement. One of the key goals is to reduce greenhouse gas emissions by at least 55 % by 2030 compared to 1990 levels and to achieve climate neutrality by 2050 [1]. A major hurdle on this path is the transport sector, which accounts for around 25 % of CO_2 emissions in the EU [2]. Heavy-duty vehicles play a key role, as they cause around a quarter of these transport-related emissions. The EU has therefore introduced CO_2 reduction targets for new trucks: a reduction of 15 % by 2025 and 30 % by 2030 compared to 2019 [3]. Electrified trucks are a promising solution for achieving these goals.
In Europe, which is increasingly facing climate change challenges, the energy sector has taken on a central role in the transition to a sustainable future. The vision of an emission-free energy system is clear: wind turbines that capture the power of the wind and solar panels that capture the sun's energy symbolize the hope of a clean energy future. Nevertheless, behind this idyllic image lies a complex reality that challenges the existing energy sector: How can a system historically based on stable and predictable energy generation, through primarily fossil and nuclear power plants, integrate the volatile and weather-dependent characteristics of renewable energy?
The answer lies in a term that is becoming increasingly important: flexibility.
The energy flows followed a linear pattern: large power plants generate electricity transported to consumers through a widely ramified grid [4]. This system was stable but rigid - little adapted to the dynamics of a rapidly changing energy sector. The emergence of renewable energies such as wind and solar power has changed this initial situation. These renewable energy sources are not only emission-free but also decentralized, volatile, and not adapted to the electricity demand but to the respective local weather conditions.
This volatile characteristic of renewable energy sources is where flexibility comes in - the ability of an energy system to adapt quickly and efficiently to changing conditions. Flexibility can occur in various forms: on the generation side, through rapid adaptation

of production [5]; in the grid, through storage technologies [6], adaptation of transmission and distribution grids [7]) and sector coupling [8]; or on the consumption side, through time-shiftable loads [9].
The electrified trucks of the future offer the potential for emission-free logistics and a resource for making the energy system more flexible on the consumption side. Their large battery capacities and predictable downtimes make them an ideal resource for flexibility services.
Through smart charging and vehicle-to-grid (V2G) technologies, battery-powered vehicles can serve as mobile energy storage units to ensure grid stability within a bidding zone and also on the electricity market [10, 11] and to minimize the use of fossil/thermal power plants for redispatch measures [12].
The targeted control of vehicle charging and discharging processes can reduce the need for redispatch measures on the generator side, for example, through expensive gas-fired power plants, and lower the operating costs of the energy system [12, 13]. Therefore, this flexibility in the energy sector can be used in various ways.
In summary, flexibility improves the integration of renewable energies, can avoid the use of emission-intensive and often expensive thermal power plants, relieves grids within a bidding zone and in electricity trading, and can be used for redispatch measures [9–12].
Austria, in particular, faces specific challenges and opportunities in the energy sector. The high proportion of renewable energies in the electricity mix, particularly from wind and solar power in the east of the country [14, 15], and Austria's central, strategic location in European electricity trading [16] make the country an ideal testing ground for innovative flexibility solutions [17]. Electrified trucks could play a key role in fully exploiting the potential of renewable energies and ensuring the grid's stability.
The modeling and simulation of the flexibility potential of electrified truck transport in the Austrian energy system in this thesis open up the possibility of identifying new synergies between the transport and energy sectors and developing innovative solutions for the challenges of the energy transition to contribute to the integration of renewable energies, the reduction of grid bottlenecks and redispatch measures, as well as to minimize fossil power plant use and should thus contribute to the achievement of international, national and European climate targets.

1.2 Research question

The successful integration of renewable energy sources and stabilizing energy grids will increasingly require flexibility, particularly on the demand side. Environmentally friendly and low-emission solutions are advantageous in this context. This thesis will examine one such solution for its potential flexibility. The research question arises from the motivation to utilize electrified commercial transport as a flexible resource in the energy sector in the future. Additionally, it addresses the necessary actions needed to enhance the integration of renewable energies into existing electricity markets:

(i) How is the flexibility of the charging power of battery electric trucks (BETs) distributed throughout Austria regarding time and location?
(ii) Can this flexibility be used reliably?

1.3 Structure of the thesis

The structure of this thesis is organized as follows: First, Chapter 2 discusses the current state of research in the field of flexibility in battery electric vehicles (EV). It also highlights the contributions this thesis makes to the existing research. Next, Chapter 3 provides a detailed functional and mathematical description of the model, along with necessary explanations for the spatial resolution employed. Additionally, it outlines the model implementation, the assumptions made, and the input data utilized.
Following that, Chapter 4 presents all the results obtained from the simulations conducted with this model. In Chapter 5, the research questions are answered based on the findings from Chapter 4. Finally, the concluding section, Chapter 6, reflects on the methodology and results, addressing the limitations of the modeling. It also suggests possible further developments and applications for the model.

2 State-of-the-Art and progress beyond

This chapter provides essential background information and state-of-the-art research relevant to this thesis. It outlines the essential state of knowledge while examining the flexibility potential of electrified heavy-duty vehicle (HDV) transportation to improve understanding of the core topic. First, the background of flexibility potential and its significance for the energy sector is discussed. It then evaluates related and relevant work that has already addressed this topic and assesses its relevance to the research question of the thesis. Finally, the contribution of this thesis is presented.

2.1 Flexibility in the electricity sector

2.1.1 Importance of flexibility

Flexibility in the electricity sector describes the ability of the energy supply system to compensate for imbalances between electricity supply and demand. In this context, flexibility can be required and effective in the short term (seconds to minutes) or the long term (hours to days or weeks). Flexibility is generally evaluated by its response time, capacity, and cost-effectiveness [18].
This flexibility is crucial to ensure a stable electricity supply, especially because of the increasing expansion and integration of volatile renewable energy sources such as wind and solar. Renewable energies cause more significant fluctuations and peak loads in electricity generation, as these technologies are dependent on weather conditions and do not always run in sync with electricity demand, so renewable energies must be balanced to avoid supply outages.
Flexibility, therefore, makes it possible to cope with difficult-to-predict fluctuations caused by volatile renewable energies, which often do not coincide with electricity demand. It also plays a key role in integrating decentralized energy sources and new consumption sectors such as EVs and heat pumps, which bring additional loads to the grid and place new demands on grid stability. Without sufficient flexibility options, costly investments in conventional reserve power capacity could become necessary, seriously jeopardizing the EU's decarbonization targets.

Consequently, flexibility in the energy sector is seen as an essential component of integrating renewable energies and grid stability. Studies show that institutional fragmentation in the EU is an obstacle, while coordinated approaches could increase economic efficiency. Integrating renewable energies and grid stability requires flexibility at all system levels (from local to national) and at all time scales (from real-time operation to long-term investments) [19].
This flexibility has a key economic dimension. Flexibility mechanisms such as demand response, battery storage, and cross-sector coupling can significantly reduce grid expansion costs and expensive peak-load power plants. It allows existing infrastructure to be used more efficiently, as peak loads can be smoothed out and surplus generation can be used at times of low load [6]. Flexibility also plays a key role in integrating national European energy markets into a networked, harmonized European energy system by optimally using cross-border trading capacities and reducing bottlenecks in the grid.
To achieve a climate-neutral electricity supply by 2050, the importance of flexibility will increase even further in the coming decades, as greater electrification of the sectors and a larger share of renewable energies will inevitably place greater demands on the energy system and thus require more flexibility from the energy sector [19].

2.1.2 Demand for flexibility

The need for flexibility is growing due to the increasing integration of renewable energies, particularly wind and solar energy, which are volatile by nature. These fluctuations require mechanisms to balance supply and demand in real-time and minimize the risk of grid instability. The researchers Chyong et al. [20] emphasize that Europe's decarbonization goals would be jeopardized without sufficient flexibility options, as renewable energy sources cannot fully replace existing fossil reserve capacities. These researchers predict that the need for flexibility will grow exponentially as the share of renewable energy increases. The need for flexibility will grow at peak times and during periods of low demand when surplus energy needs to be stored or exported.
In addition to seasonal imbalances, which require long-term storage solutions such as hydrogen, power-to-X, or long-term storage technologies, short-term daily fluctuations must be balanced out in real-time. Especially in extreme weather conditions, when renewable energies are not sufficiently available in some regions, the need for flexibility increases. According to Chyong et al. [20], the demand for battery storage alone, as flexibility for the energy supply, is expected to increase 10-fold compared to current capacities by 2050, especially in countries with a high proportion of solar energy. This will require considerable investment in technologies and infrastructure. Increased regional cooperation in Europe is seen as necessary to promote cross-border trade and the shared use of flexibility options.

Flexibility is necessary not only to keep the electricity supply stable but also to minimize the costs of the energy system. This includes using storage systems, demand response, and cross-border energy trading to mitigate peak loads and efficiently use renewable surpluses [20].

2.1.3 Flexibility options

The literature identifies several technologies and approaches for providing flexibility. These are divided and classified into various supercategories.
There are storage technologies such as battery storage, power-to-gas, and pumped storage power plants, which can increase the use of renewable energies and minimize the need for new capacities through long-term storage and thus flexibility [6].
Another option is sector coupling, which links the electricity, heat, and gas sectors to increase flexibility. Technologies such as power-to-heat offer flexibility by converting electricity into other forms of energy in order to compensate for the high fluctuations in renewable energies [8].
One prevalent option today for increasing flexibility in energy generation is the use of conventional power plants, such as gas-fired and hydrothermal power plants. Huber et al. [5] asserts that integrating these plants into larger transnational grids reduces the need for flexibility compared to smaller regional grids, as fluctuations in energy production can be better balanced, especially with a high proportion of wind power. However, gas-fired power plants are not aligned with the European Union's goal of achieving CO_2 neutrality by 2050, making them unsuitable as a long-term solution for enhancing flexibility.
Grid-side solutions also increase flexibility. According to Poncela et al. [7], in addition to storage technologies, investments in the expansion of transmission grids are significant to avoid congestion and increase grid efficiency. The paper underlines the importance of coordinated European action to promote grid flexibility through innovative technologies and regulatory frameworks. In addition to expanding transmission grids, these can also include intelligent grid control systems such as smart grids. These smart grids offer opportunities to increase grid flexibility through their ability to communicate and optimize in real-time [21].
Beyond generator-side and grid-side measures, load-side options are also integral to increasing flexibility. Forouli et al. [9] highlight that load-side flexibility is essential for balancing fluctuations in energy production. This flexibility can be achieved by adjusting electricity consumption in industries and households based on price signals or grid requirements. Simulation results from Lu et al. [22] reveal that a dynamic pricing algorithm, which takes into account consumer load profiles, wholesale price fluctuations, and the profitability of electricity suppliers, can help balance energy supply and demand while improving the reliability of electricity systems. Moreover,

electrified transportation can serve as a source of flexibility through vehicle-to-grid (V2G) technologies [23], as well as by leveraging the charging flexibility of electric vehicles (EVs). This involves dynamically adjusting charging times and power levels to ease the load on the power grid or to make optimal use of available renewable energy [24]. This form of flexibility will be a primary focus of the investigations during this thesis.

In general, studies on flexibility in the energy sector emphasize the need for a balanced portfolio of flexibility measures to promote the integration of renewable energy. This includes the interdependencies between storage solutions, grid-side flexibility, and demand response [18]. In summary, flexibility in the electricity sector is a key prerequisite for integrating renewable energies and ensuring grid stability. Demand is growing due to decarbonization targets and electrification. A combination of technical, market-related, and political measures can provide flexibility and enable the transition to a sustainable energy system.

2.2 Flexibility potential of electrified trucks

Due to the relevance of the expansion of renewable energies in Europe, more and more scientific studies are dealing with flexibility potential. In the following, this paper focuses on the flexibility potential of electrified truck transport in Austria. However, studies are presented here that represent the latest state of research in the somewhat broader field of flexibility potential through electrified vehicles, as there is a lack of studies in the particular field of electrified trucks in Austria.
In their paper "Analyzing the Charging Flexibility Potential of Different Electric Vehicle Fleets Using Real-World Charging Data", the researchers Barthel et al. [25] analyze the flexibility potential of EV fleets (three different vehicle fleets are examined: pool vehicles of office employees, public authority and a logistics company) based on real charging data and show that logistics fleets have the highest charging flexibility potential. In the data analysis, logistics sites are particularly well suited, as logistics fleets show the most homogeneous charging profile and the highest flexibility potential, making them ideal for smart charging and grid support. Public authority pool vehicles have less predictable charging profiles, which limits their flexibility. Time and power-related flexibility behaviors are analyzed by examining average charging power per charging session, plug-in duration, and charging speed parameters. Higher charging speeds and longer parking times significantly increase the flexibility potential.
This study concludes that charging flexibility depends on fleet usage and that logistics fleets offer considerable opportunities for grid stabilization due to their consistent charging profiles and long-standing times.

Another study, "Flexibility Potential of Smart Charging Electric Trucks and Buses", by researchers Will et al. [26], examines how BETs and buses in Germany can provide up to 23 GW of flexibility through smart charging by 2040. A bass diffusion model is used to simulate the charging requirements of electric heavy-duty vehicles in five typical use cases (long-distance freight transport, regional distribution transport, urban logistics, public buses, and construction site vehicles). The vehicles' time availability and charging behavior are analyzed to quantify the flexibility potential. The results show that these vehicles' charging processes can contribute to grid stability and reduce operating costs. It is emphasized that access to flexibility markets for operators of heavy vehicle fleets should be simplified and automated, with regulation and market mechanisms playing a key role, as smart charging approaches can also reduce operating costs for vehicle fleets due to the existing flexibility potential. The need for coordinated planning between energy markets, grid operators, and fleet management is also emphasized.
In summary, this study shows that electric trucks and buses offer significant flexibility potential for the energy system, primarily through smart charging approaches. This flexibility supports the integration of renewable energies, helps avoid grid bottlenecks, and reduces costs. The authors argue for greater political and regulatory support to use these opportunities effectively.
The paper "Flexibility Potential of Aggregated Electric Vehicle Fleets to Reduce Transmission Congestions and Redispatch Needs: A Case Study in Austria" by the researchers Loschan et al. [27] examines the flexibility potential of aggregated EV fleets in Austria. It analyzes how these fleets can help to reduce congestion in the transmission grid and reduce the need for redispatch measures by evaluating flexibility based on simulation. The vehicles are examined in realistic scenarios, considering mobility behavior, charging profiles, and grid requirements. The focus is on using V2G technologies and their contribution to grid stabilization and economical operation.
The main findings of this study are that EV fleets can make significant contributions to grid flexibility, especially at peak load times or with a high proportion of renewable energies, if the fleets are geographically close to the bottleneck points, as this maximizes their effectiveness. This flexibility leads to lower redispatch costs and more efficient use of grid capacities. When integrating this flexibility, it is crucial that there is suitable coordination between grid operators and EV aggregators (EV aggregators are service providers that bundle several EVs into one unit and coordinate their collected charging or discharging flexibility to make it available on energy markets or in the electricity grid) in order to create low barriers for customers in the congestion management market. In addition, regulatory incentives are needed to encourage investment in charging infrastructure and V2G technologies.
In summary, this paper focuses on a simulation-based analysis of flexibility in Austria to analyze the application of flexibility of EV fleets in the redispatch market, highlighting the importance of geographical proximity between the EV fleets with flexibility potential and the congestion points.

2.3 Own contribution

The potential of demand-side flexibility provided by electrified trucks is generated in this thesis using a bottom-up model and then presented both over time and in terms of spatial distribution at NUTS3 level in Austria. This thesis thus focuses on an initial assessment of the geographical distribution of the flexibility potential. The necessary breaks and energy demand are, and the resulting flexibility potential of different regions and times is calculated using detailed, synthetically generated routes and individually starting truck fleets.

(i) Modeling of international truck traffic affecting Austria as a bottom-up model based on synthesized routes and individual, Gaussian normally distributed starting truck fleets.
(ii) Application of the model to estimate the temporal and spatial distribution of the flexibility potential of electrified truck transport in Austria.
(iii) Analysis of the model to assess possible sensitivity to the flexibility potential.
(iv) Simulation and evaluation of the influence of limited installed capacities on the flexibility potential of electrified truck transport in Austria.

3 Methodology

This chapter outlines the methodology, the mathematical formulation of the model, and the input data utilized.
Section 3.1 details the geographical resolution applied and describes the necessary data for the model, along with the preprocessing steps taken. The subsequent section, Section 3.2, provides an overview of the model's functionality. Section 3.3 presents the normal distribution used in the model and defines the flexibility incorporated to address the research question.
The Section 3.4 that follows provides the nomenclature for the variables and parameters, calculations for determining the truck fleets, calculations for the required breaks on individual routes, and calculations for assessing the resulting flexibility.
In the following section, Section 3.5, the software utilized to implement the model and graphics is briefly described and named. The final section, Section 3.6, contains all the input data used in the study. All parameters are generally denoted with uppercase letters, while all variables are represented with lowercase letters.

3.1 Spatial distribution

In addition to presenting the NUTS3 regions used for the spatial classification, this section describes how the various datasets are processed so that they can be used as data for the model.
The data basis for this work is a dataset by Speth et al. "Synthetic European road freight transport flow data based on ETISplus" [28] from 2021, which shows the truck routes through Europe with the corresponding forecast truck traffic for the years 2010, 2019 and 2030, as well as traffic count data from ASFINAG (Autobahnen- und Schnellstraßen-Finanzierungs-Aktiengesellschaft; Freeway and federal highway financing stock corporation) for Austria [29].
The traffic count data is collected using overhead detectors (a combination of ultrasound, passive infrared, and radar detectors [29]) and induction loops on the Austrian freeway and highway network.

3.1.1 NUTS3 regions

The local classification of data and results takes place in Nomenclature of Territorial Units for Statistics (NUTS) regions [30].
This NUTS classification system, developed by the European Union (EU), divides EU countries into three different levels.
Level 3 (NUTS3), the most detailed level, is selected for further consideration. In addition to the territorial administrative division of the individual countries, the regions are classified according to the number of inhabitants.
The NUTS3 level is defined from a minimum of 150,000 to 800,000 inhabitants per subdivided region [31].
The classification and divisions of the NUTS3 regions in Austria, as applicable in 2024, will serve as the foundation for this thesis. This information is illustrated in Figure 3.1, Table A1, and Table A2.

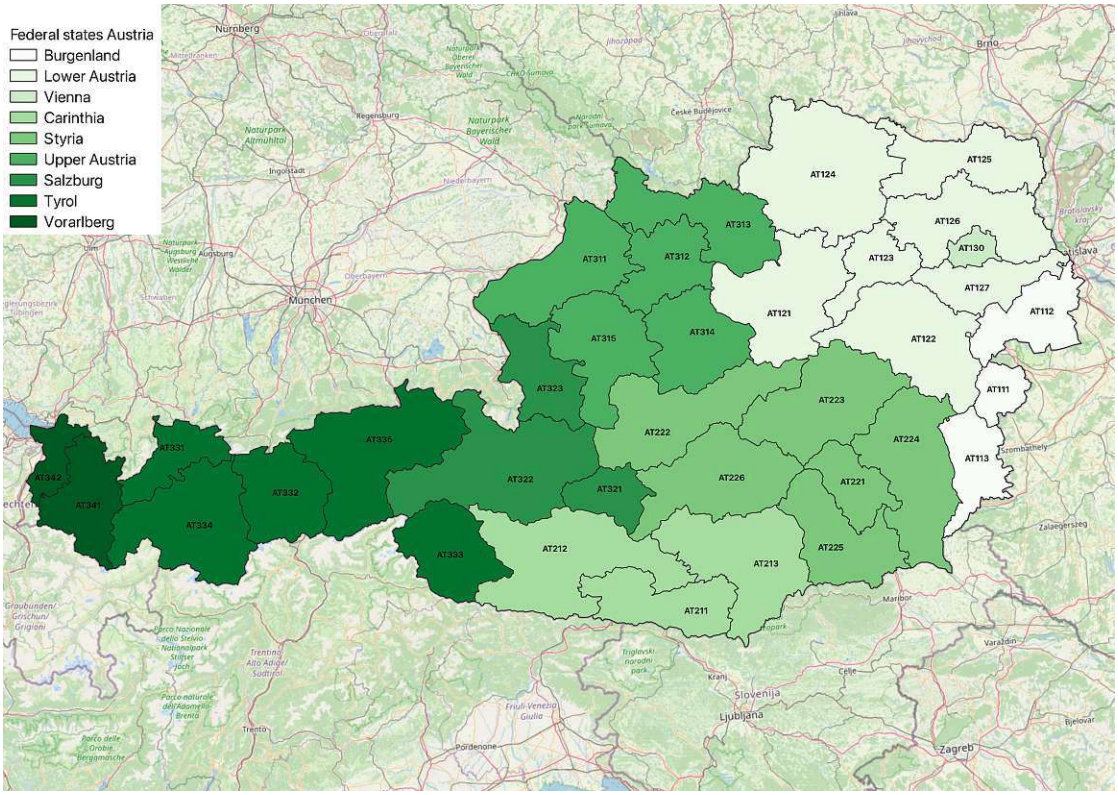

Figure 3.1: NUTS3 regions Austria

3.1.2 Datasets preprocessing

Before utilizing the dataset by Speth et al. [28], all truck routes r are filtered to include only those that pass through Austria. A truck route r consists of edges E, each formed by two nodes N (Figure 3.2). For half of these truck routes r, the edges are arranged in the incorrect direction of travel. Specifically, in this scenario, the route begins with E_i and concludes with E_1, despite E_i being closer to the destination. Since the direction of travel is crucial for the model and for accurately determining locations, the direction of these truck routes is corrected by reversing the order of the edges.

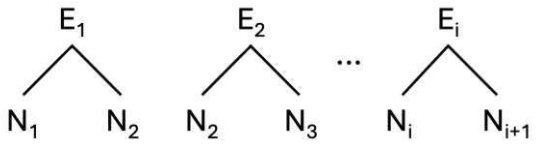

Figure 3.2: Theoretical basic structure of a truck route on the E-roads (European freeways and national roads)

In the dataset by Speth et al. [28], there is a single edge for each pair of nodes. This indicates that the edges represent only one direction of travel. However, the routes associated with these edges are applicable in both directions. Additionally, the nodes of the respective edges are not always in the correct order, even for routes where the edges are arranged correctly in the unprocessed dataset (see Figure 3.3 and Figure 3.2). Node N_1, which is the first point on the E-road from the direction of the start, is in second place on the example route from Mittelburgenland to Freising. For the edge E_1, the nodes N_1 and N_2 would have to be swapped. On this route, 53 of 91 edges have swapped nodes.
In order to determine an exact location, it is necessary to extend the edge data by incorporating the edges corresponding to the respective missing directions of travel. Additionally, the node pairs N_i and N_{i+1} associated with the edges E_i of the individual routes r must be arranged in the correct sequence. Since this model only considers locations at the NUTS3 level, the extension and correction of the data are not included in this analysis.

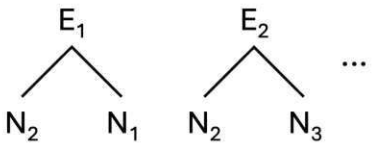

Figure 3.3: Example of the actual structure of a specific route

Since this dataset, with the European truck routes, only contains the number of trucks per year on the respective route r, but here the time steps should ultimately be in 15 min intervals, the nodes N are linked to the ASFINAG counting stations. This is implemented by assigning the nearest (air-line distance) ASFINAG counting station to each node N (the nodes and counting stations can be seen in Figure 3.1.2). This allows the routes to be extended with actual truck counts at the respective locations so that the two datasets combined contain the European truck routes, which include Austria on the routes (national, import, export, and transit routes), with the number of trucks in trucks per 24 h. The combined dataset is referred to below when the data set is mentioned.

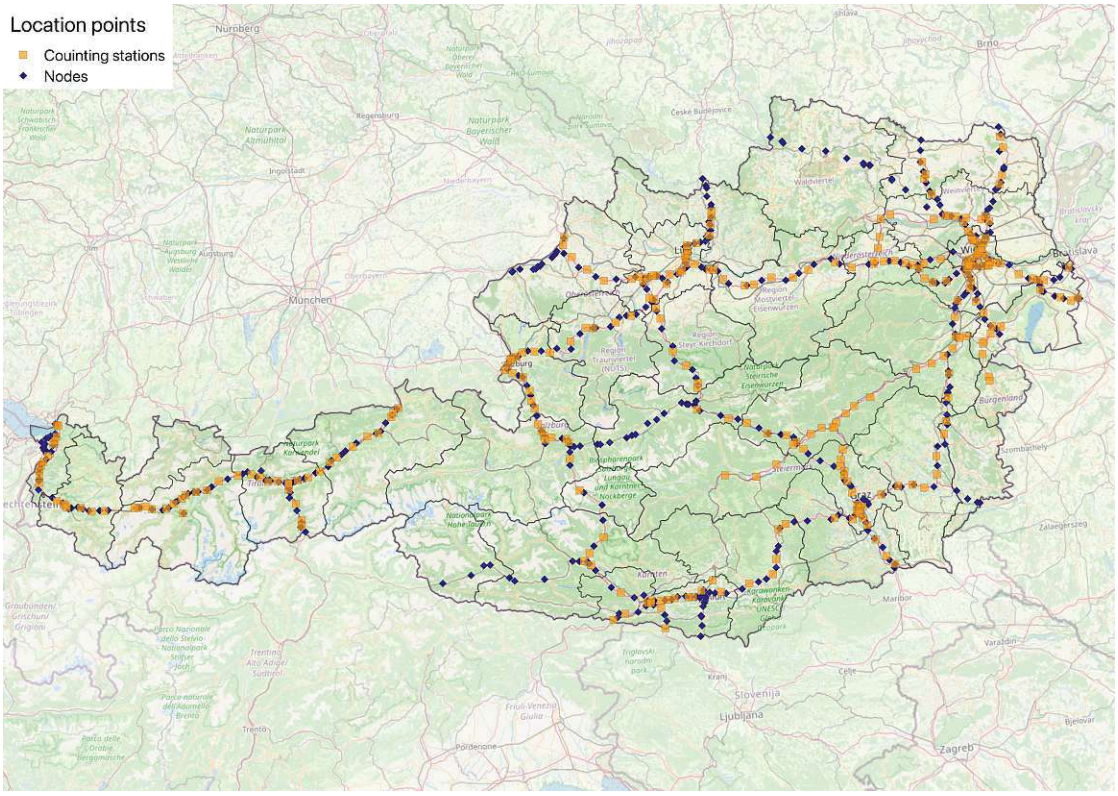

Figure 3.4: Austria map with nodes and counting stations

3.2 Model functionalities

The model is constructed using a bottom-up approach, as illustrated in Figure 3.5. With the focus on the mathematical model, in the first block, titled "BET Fleet Simulation," individual battery-electric truck fleets are simulated separately across all the available routes in the dataset. The results of these simulations are then used to calculate the flexibility potential for different regions and time periods in the subsequent blocks. The BET fleet simulation determines the necessary break locations and the energy consumed since the last charge based on the available truck routes. This is combined with data on truck counts at specific locations, normally distributed start times, and statutory driving times.
Consequently, the model calculates the minimum required charging power, denoted as p_{min}, which is needed to fully charge all plugged-in BETs in the specified region. Additionally, it determines the maximum available charging power, p_{max}, for each NUTS3 region and time step T (referred to as the "p_{min} and p_{max} calculation" block).
In the following block, labeled "P_{limit} calculation", the limits for installed capacities are established. This includes $P_{Limit_{min}}$, which represents the minimum installed capacity required to fully charge all plugged-in BETs. Conversely, $P_{Limit_{max}}$ refers to the maximum level of installed capacity that allows all connected BETs to be charged at their maximum power at all times.
Finally, the flexibility in terms of time steps and regions is analyzed and presented in the data analysis section. The flexibility of charging power is indicated by the values p_{min}, p_{max}, and the reserve power Δp.

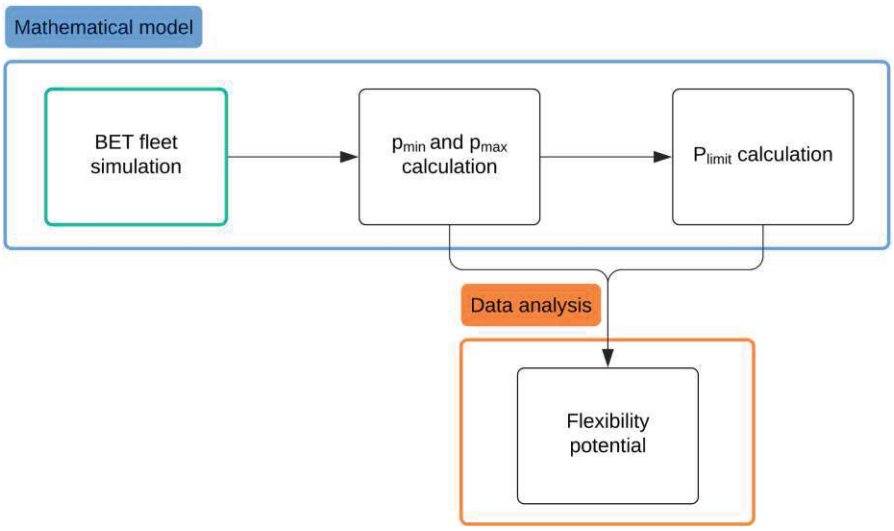

Figure 3.5: Overview of the Methodology

The Figure 3.6 illustrates the basic structure of the BET fleet simulation, which is part of the mathematical model. Initially, the combined dataset (referred to as the "Dataset" block) described in Subsection 3.1.2 is utilized to calculate the number of BETs per 24 h ($r_v(day)$), based on the day of the week, month, and route (see the block titled "BET calculation r_v" in Figure 3.6). The total number of BETs per route ($r_v(day)$) is divided to determine the number of BETs per fleet ($r_i(day)$) on that route, which depends on the value of $r_v(day)$.
For each fleet i, a separate, normally distributed start time is generated ("BET fleet calculation r_i"). Once the start time is generated ("Start time generation"), the BET fleet begins its journey on the respective route ("Simulate fleet on route"). The required breaks are calculated by the legally applicable driving times, break times, speed limits, and night driving bans in Austria ("Breaks calculation b_f" where b_f denotes the number of breaks). This calculation relies on comprehensive route information from the combined dataset, which includes the NUTS3 start region, the distance from the start region to the first edge on the E-road, the route on the E-road represented by a series of edges (as depicted in Subsection 3.1.2 and Figure 3.2), as well as the distance from the last edge on the E-road to the destination region and the corresponding NUTS3 destination region.
For each fleet break, information such as the start and end times of breaks, location, number of trucks, and the energy consumed since the start or the last break (if applicable) is recorded. This information is also stored for fleets arriving at their destination. At the destination, the arrival time of the fleet is crucial. Suppose the fleet arrives before a specific time T_{dest} (which allows the BET to take a short break at the destination, denoted as $T_{short_{dest}}$, and continue its journey on the same day). If the fleet arrives after the specific time T_{dest}, the pause time at the destination is extended until night (represented by the last block "Plugged-in..."). Using the stored information, values for p_{min} and p_{max} are calculated or aggregated for each NUTS3 region and time step T. This enables the presentation of the flexibility of charging power per NUTS3 region and time step.

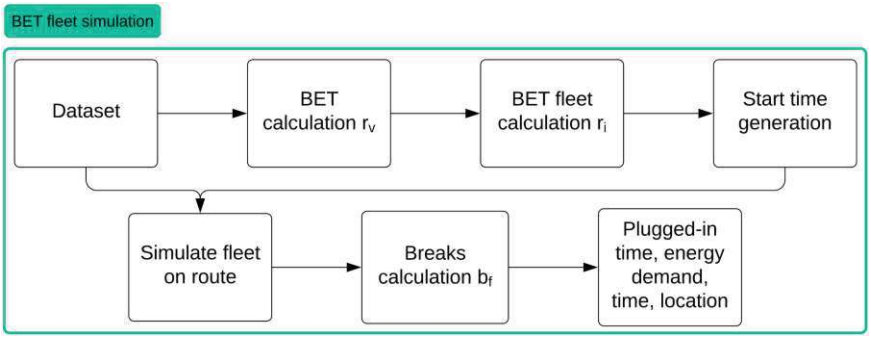

Figure 3.6: Overview of the simulation of truck fleets

3.3 Mathematical framework

3.3.1 Gaussian normal distribution

A Gaussian normal distribution is used to generate the start times $\widetilde{t}^{start}_{r_i(day)}$ of the individual truck fleets as the sum of a large number of independent and identically distributed random variables is approximately normally distributed [32]. The symmetrical, bell-shaped distribution is modeled as a mean value μ around a time that does not fall within the time window of the night driving ban.
Due to the night driving ban in Austria [33], the bell curve may be truncated at the sides, depending on the selected mean value μ and the standard deviation σ, and the symmetry is lost.
The density function of the normal distribution used here is given by Equation 3.7.

3.3.2 Definition of the flexibility potential

The following definition of the flexibility potential is used in this thesis. The charging power's flexibility potential Δp (see Equation 3.22, also called reserve power) is divided into time steps T.
On the one hand, the minimum charging power p_{min} required to fully charge the respective BET in the specified time $t_{b_{f_{period}}}$ from plug-in to plug-out is considered. On the other hand, the maximum charging power p_{max} that is technically possible, summed over the number of connected BETs in the specified time $t_{b_{f_{period}}}$ and their maximum possible charging power. The range between p_{min} and p_{max} (Figure 3.7) represents the usable flexibility potential of the charging power in the respective time step T.

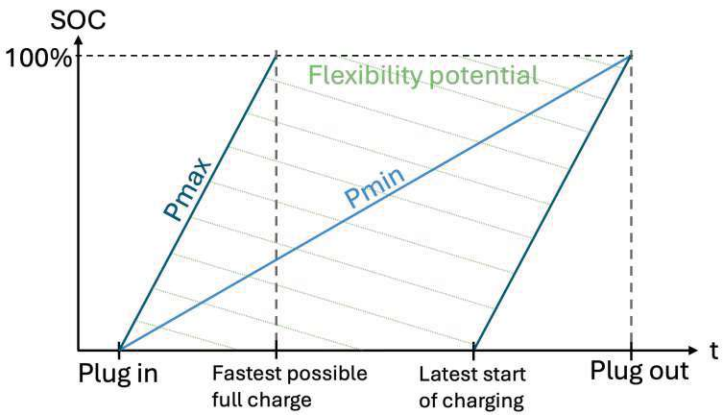

Figure 3.7: The flexibility potential of a BET

3.4 Mathematical model

This chapter mathematically describes the model already described in its functionality in Section 3.2. It is divided into three subsections in addition to the nomenclature. Firstly, the calculation of the number of trucks or fleets in Subsection 3.4.2 is described mathematically, then the calculation of the start time, breaks as well as the corresponding energy requirements in Subsection 3.4.3 and finally, the calculation of the flexibility resulting from the previous calculations in Subsection 3.4.4.
The construction of the mathematical model stipulates that breaks are only taken due to the specified maximum driving time of a truck driver in one go $T_{drive\_time\_limit}$ or the night driving ban in Austria and not due to an empty battery of the BET. It is assumed that the range of the BET is sufficient to cover the maximum distances in one go without intermediate charging. It is also assumed that the charging power of a BET is sufficient for the energy consumed during the driving time $T_{drive\_time\_limit}$ to be fully recharged during the minimum break time T_{short}.

3.4.1 Nomenclature

Sets		
E	All edges	$index: e$
N_n	All nodes	$index: n$
R	All routes	$index: r$
T	Time steps	$index: t$
Parameters		
C_{avg}	Average consumption of a BET	kW/km
C_{batt}	Battery capacity of a BET	kWh
$P_{max\_chargespeed}$	Maximum battery charging power of a BET	kW
$P_{Limit_{min}}$	Maximum of p_{min} within a certain region and period of time	MW
$P_{Limit_{max}}$	Maximum of p_{max} within a certain region and period of time	MW
$T_{start_{night\_ban}}$	Start of the night driving ban	h
$T_{end_{night\_ban}}$	End of the night driving ban	h
$T_{day_{max}}$	Maximum daily driving time per truck driver	h
$T_{drive\_time\_limit}$	Maximum driving time in one go	h

Table 3.1: Sets and parameters

Parameters		
T_{short}	Short legally prescribed charging pause	h
T_{long}	Long legally prescribed charging pause	h
$T_{short_{dest}}$	Short break at destination	h
T_{dest}	Time limit after which the truck fleet r_i takes a long break at the destination	h
V_{e-road}	Average speed driven on E-road	km/h
V_{others}	Average speed driven on all other roads	km/h
V_{limit}	Limit above truck fleet r_v is divided into smaller fleets	$N/24h$
$V_{divider}$	Divider if the truck fleet r_v exceeds the limit V_{limit}	
X_{BET}	Share of BETs in the total number of trucks	
Variables		
b_f	Number of breaks taken with $\{b_1, ..., b_F\}\ \epsilon\ b$	N
d	Distance driven	km
$d_{e(n_g)}$	Distance of the edge e where the corresponding node n_g is the second node	km
e_{bet}	Energy consumption of a BET within the fleet r_i	kW
p_{min}	Minimum charging power summed locally and over time	MW
p_{max}	Maximum charging power summed locally and over time	MW
$r_v(day)$	Number of BETs per route depending on the weekday	$N/24h$
$r_{v_{avg}}(day)$	Number of trucks at ASFINAG counting station with smallest $r_{v_{avg}}(week)$ value, on the respective route r, depending on the weekday	$N/24h$
$r_{v_{avg}}(week)$	Number of trucks per week at ASFINAG counting station with smallest $r_{v_{avg}}(week)$ value, on the respective route r	$N/24h$
$r_{v_{avg}}(year)$	Forecasted average number of trucks per route r for the respective year	$N/year$
$r_i(day)$	Number of BETs in fleet i per route r with its own Gaussian normally distributed start time depending on the weekday	$N/24h$
SoC	State of charge of the truck battery	%
t_{b_f}	Start time of the charging break	h
$t_{b_{f_{period}}}$	Period of the respective charging break	h
$t_{b_{f_{period}}}(day)$	Period of the respective charging break on a specific day	h

Table 3.2: Parameters and variables

Variables		
$t_{r_i(day)}$	Time step of a truck fleet on a route r_i with its own start time	h
$t^{sum}_{r_i(day)}$	Sum of driving time + break time per truck fleet on a route r_i	h
$\widetilde{t}^{start}_{r_i(day)}$	Gaussian normally distributed start time of a truck fleet r_i	h
$t_{n_g}(\widetilde{t}^{start}_{r_i(day)})$	Time at a specific node n_g with $\{n_1, ..., n_G\}\ \epsilon\ n$ for the respective truck fleet r_i with the start time $\widetilde{t}^{start}_{r_i(day)}$	h
$t_{e(n_g)}$	Drive time required to drive along a specific edge e	km
t_{before}	Drive time from the start of the specific route to the first node on the E-road n_1	km
t_{after}	Drive time from the last node of the E-road n_G of the specific route r to the Destination	km
$t_{n_g}(\widetilde{t}^{start}_{r_i(day)})$	Drive time of a specific fleet on a specific route r_i with a specific start time $\widetilde{t}^{start}_{r_i(day)}$ from start to a specific node n_g	km
$t_{drive\_time_{total}}$	Total drive time of a truck fleet r_i	h
$t_{drive\_time_{n_g}}(day)$	Drive time of a truck fleet r_i of one day up to the considered node n_g	h
$t_{long_{dest}}$	Long break overnight at the destination	h

Table 3.3: Variables

3.4.2 Truck fleet

The number of BETs per route and depending on the day $r_v(day)$ is first required so that the number of trucks in the fleet i, and therefore $r_i(day)$, can be calculated. As described in Subsection 3.1.2, this is combined from the forecasts by Speth et al. [28] and the traffic count data of ASFINAG [29]. Equation 3.1 shows the calculation.
The trucks $r_{v_{avg}}(day)$ counted on a particular day are divided at the counting station with the lowest number of trucks counted in the weekly average $r_{v_{avg}}(week)$ on the route in question by the value of trucks in the weekly average $r_{v_{avg}}(week)$ of the counting station in question ($r_{v_{avg}}(day)$ and $r_{v_{avg}}(week)$ come from the same counting station).
This results in a relative value that differentiates the number of trucks per route depending on the day of the week. This factor is multiplied by the forecast of trucks per route (which is only available as an annual forecast), which originates from Speth et al. [28] so that the number of trucks per route can be differentiated by day of the week. The result is then multiplied by the forecast rate for BETs X_{BET} so that $r_v(day)$

finally represents the number of BETs per route depending on the day of the week per 24 hours (see Equation 3.1).

$$r_v(day) = \frac{r_{v_{avg}}(day)}{r_{v_{avg}}(week)} \cdot \frac{r_{v_{avg}}(year)}{365} \cdot X_{BET} \tag{3.1}$$

$$\forall\{r_1(day), ..., r_I(day)\}\epsilon r, \forall r\epsilon R$$

The determination of the number of trucks per fleet and route $r_i(day)$ is, as can be seen in Equation 3.2, dependent on the limiting parameter V_{limit}. This parameter is introduced because the total number of BETs per route and 24h depending on the day $r_v(day)$ is available in floating point numbers. How many BETs a fleet contains should be clearly defined, which should then receive a normally distributed start time to increase the reference to reality. The case distinction can be seen in Equation 3.2.
If the limit V_{limit} is not reached, then $r_i(day) = r_v(day)$ and there is only one fleet ($i = 1$) on this route on the respective day with a normally distributed start time and the BET fleet size of $r_i(day)$.
If the limit V_{limit} is reached or exceeded, the total number of BETs per route and 24h depending on the day $r_v(day)$ is divided by the x, which is rounded down to the nearest integer value (floor function). The x is calculated by dividing the $r_v(day)$ by the parameter $V_{divider}$. The number of BET fleets on this route on the respective day with their own normally distributed start times i then corresponds to the x rounded down to the nearest integer value ($i = \lfloor x \rfloor$). The individual fleets here consist of $r_i(day)$ BETs.

$$r_i(day) = \begin{cases} r_v(day), & r_v(day) < V_{limit},\ i = 1 \\ \frac{r_v(day)}{\lfloor x \rfloor}, & r_v(day) \geq V_{limit},\ x = \frac{r_v(day)}{V_{divider}},\ \lfloor x \rfloor = max\{n\epsilon\mathbb{Z} | n \geq x\},\ i = \lfloor x \rfloor \end{cases} \tag{3.2}$$

$$\forall\{r_1(day), ..., r_I(day)\}\epsilon r, \forall r\epsilon R$$

3.4.3 Start, breaks and destination

The underlying dataset distinguishes between route sections on E-roads (all these route sections are connected via edges and these consist of a pair of nodes (Subsection 3.1.2) - E-roads consisting of freeways and federal highways), as well as a route sections between the start and the first node on the E-road and the last node on the E-road and the destination (all other roads such as country roads or city streets). The dataset provides a route section length d for all these individual points. Combined with the two speed parameters V_{e-road} and V_{others}, this results in the corresponding drive times for covering this route section distance d, as seen in the following equations.

In the following mathematical model, the use of these equations to calculate times from the route section lengths given in the dataset is taken as given.
The distance between the start and the first node d_{before} or the last node and the destination d_{after} is only available as a route length value without further subdivision. Therefore, before and after the E-roads, a necessary break (if $t > T_{drive\_time\_limit}$) is only stored as the location of the NUTS3 region of the start or destination and the corresponding energy consumption (see Equation 3.18). However, apart from a few transit routes that start or end in regions outside Europe with weak infrastructures, such as eastern Russia, this does not occur.
The Equation 3.3 is required to calculate the required drive time for one edge $t_{e(n_g)}$. For this purpose, the distance $d_{e(n_g)}$ of the edge is used, where the node n_g is the second node N_2 (Subsection 3.1.2) and this is divided by the speed on the E-road V_{e-road}.

$$t_{e(n_g)} = \frac{d_{e(n_g)}}{V_{e-road}} \tag{3.3}$$

To calculate the drive time before or after the E-road, the corresponding Equation 3.4 is used, with the specified speed on all other roads as an E-road V_{others}. The respective distance of the route before d_{before} or after d_{after} the E-road is divided by the speed V_{others}.

$$t_{before} = \frac{d_{before}}{V_{others}} \tag{3.4}$$

$$t_{after} = \frac{d_{after}}{V_{others}}$$

Equation 3.5 is required to calculate the time from the start of a fleet up to a specific node n_g, which is needed for further calculation of the breaks. Here, the start time $\widetilde{t}^{start}_{r_i(day)}$ of the respective fleet (Equation 3.7) is added to the corresponding drive time t_{before} of this route and the sum of all drive times of the edges up to this node n_g.

$$t_{n_g}(\widetilde{t}^{start}_{r_i(day)}) = \widetilde{t}^{start}_{r_i(day)} + t_{before} + \sum_{g=1}^{g} t_{e(n_g)} \tag{3.5}$$

The calculation of the total drive time of a route $t_{drive\_time_{total}}$ in Equation 3.6 is the addition of the drive time before t_{before} and after t_{after} the E-road and the total drive time on the E-road $\sum_{g=1}^{G} t_{e(n_g)}$.

$$t_{drive\_time_{total}} = t_{before} + \sum_{g=1}^{G} t_{e(n_g)} + t_{after} \tag{3.6}$$

$$\forall\{e(n_1),...,e(n_G)\}\epsilon e, \forall\{n_1,...,n_g\}\epsilon n$$

Start time

The start time calculation is a Gaussian normal distribution, which is limited by the night driving ban, in the time from the start of the night driving ban ($T_{start_{night\_ban}}$) to the end of the night driving ban ($T_{end_{night\_ban}}$). During this period of the night driving ban, no trucks are allowed to drive in Austria, so they are not allowed to start.
This results in the Equation 3.7 with the condition that the normally distributed start time of a fleet $\widetilde{t}^{start}_{r_i}$ must lie in the period from $T_{end_{night\_ban}}$ to $T_{start_{night\_ban}}$.

$$\widetilde{t}^{start}_{r_i(day)} \sim \mathcal{N}_{(\mu_g,\sigma_g)}, \tag{3.7}$$

$$\widetilde{t}^{start}_{r_i(day)} = \frac{1}{\sqrt{2\pi}\cdot\sigma}\cdot \mathrm{e}^{-\frac{1}{2}\left(\frac{x-\mu}{\sigma}\right)^2},$$

$$\widetilde{t}^{start}_{r_i(day)} \epsilon (T_{end_{night\_ban}}, T_{start_{night\_ban}}),$$

$$\forall\{t_{r_1(day)},...,t_{r_I(day)}\}\epsilon t, \forall t\epsilon T, \forall\{r_1(day),...,r_I(day)\}\epsilon r, \forall r\epsilon R$$

Breaks

The following conditions and calculations determine whether the respective BET fleet $r_i(day)$, with its normally distributed start time, takes a break on the route. A distinction is made in Equation 3.8 as to whether it is the first break on the journey ($b_f < 1$) or whether breaks have already taken place ($b_f \geq 1$).
Suppose the fleet has not yet paused on the journey. In that case, it is paused as soon as the time $t_{n_g}(\widetilde{t}^{start}_{r_i(day)})$ at a specific node n_g at which the fleet is currently located, minus the start time of the fleet $\widetilde{t}^{start}_{r_i(day)}$, is greater than the maximum drive time of the fleet in one go ($T_{drive\_time\_limit}$).
If one or more breaks have already been made, the end of the last break ($t_{b_{f-1}} + t_{b_{f-1_{period}}}$) is subtracted from the time $t_{n_g}(\widetilde{t}^{start}_{r_i(day)})$ at a specific node n_g where the fleet is currently located, instead of the start time of the fleet $\widetilde{t}^{start}_{r_i(day)}$.

$$T_{drive\_time\_limit} < \begin{cases} t_{n_g}(\widetilde{t}^{start}_{r_i(day)}) - \widetilde{t}^{start}_{r_i(day)}, & b_f < 1 \\ t_{n_g}(\widetilde{t}^{start}_{r_i(day)}) - (t_{b_{f-1}} + t_{b_{f-1_{period}}}), & b_f \geq 1 \end{cases} \tag{3.8}$$

Additionally, if the daily drive time $t_{drive\_time_{ng}}(day)$ of a BET fleet r_i surpasses the maximum allowable daily drive time $T_{day_{max}}$, the fleet will be paused (Equation 3.9).

$$T_{day_{max}} < t_{drive\_time_{ng}}(day) \tag{3.9}$$

$$\forall\{r_1(day),...,r_I(day)\}\epsilon r, \forall r\epsilon R, \forall\{n()_1,...,n()_G\}\epsilon n,$$
$$\forall\{t_{r_1(day)},...,t_{r_I(day)}\}\epsilon t, \forall\{t_{b_1},...,t_{b_F}\}\epsilon t, \forall t\epsilon T$$

The start time of the charging time can be found in the Equation 3.10. This start time of the break is the time $t_{n_{g-1}}(\widetilde{t}^{start}_{r_i(day)})$ at which the fleet was at the node n_{g-1}, one node before one of the conditions of Equation 3.8 and Equation 3.9 is fulfilled.

$$t_{b_f} = t_{n_{g-1}}(\widetilde{t}^{start}_{r_i(day)}) \tag{3.10}$$

The break period for which the fleet is plugged in is differentiated between two cases (Equation 3.11). It is a short break with the length T_{short} if it is either the first break ($b_f < 1$) on the route for this fleet r_i or the length of the last break $t_{b_{f-1_{period}}}$ is greater than or equal to the break length T_{long}. It is a long pause with the length T_{long} if the length of the last pause $t_{b_{f-1_{period}}}$ is short (T_{short}).

$$t_{b_{f_{period}}} = \begin{cases} T_{short}, & b_f < 1 \vee t_{b_{f-1_{period}}} \geq T_{long} \\ T_{long}, & t_{b_{f-1_{period}}} = T_{short} \end{cases} \tag{3.11}$$

$$\forall\{r_1(day),...,r_I(day)\}\epsilon r, \forall r\epsilon R, \forall\{n()_1,...,n()_G\}\epsilon n,$$
$$\forall\{t_{r_1(day)},...,t_{r_I(day)}\}\epsilon t, \forall\{t_{b_1},...,t_{b_F}\}\epsilon t, \forall t\epsilon T$$

Night driving ban

The constraint for a break on the route due to the night driving ban can be seen in Equation 3.12. First, $t^{sum}_{r_i(day)}$ is the addition of the driving time of the BET fleet r_i for one day $t_{drive\_time_{ng}}(day)$ and the sum of the periods of all breaks taken by this fleet on this day. The constraint based on this value $t^{sum}_{r_i(day)}$ is divided into two cases.
If the number of breaks is less than or equal to one ($b_f \leq 1$) and the break taken so far is less than the break period T_{long} (which is equally important, that there has not yet been a night break), the start time of the fleet is subtracted from the start time of the night driving ban $T_{start_{night\_ban}}$. If this value is less than $t^{sum}_{r_i(day)}$, there is a night break.
In the second case, if there has already been a night break or more than one break ($b_f > 1$), the following results. If the value $t^{sum}_{r_i(day)}$ is greater than the subtraction from

the start of the night driving ban $T_{start_{night\_ban}}$ minus the start time $T_{end_{night\_ban}}$ of the BET fleet on the respective day, a night break is taken.

$$t^{sum}_{r_i(day)} = t_{drive\_time_{n_g}}(day) + \sum_{f=1}^{F} t_{b_{f_{period}}}(day), \tag{3.12}$$

$$t^{sum}_{r_i(day)} > \begin{cases} T_{start_{night\_ban}} - \widetilde{t}^{start}_{r_i(day)}, & b_f \leq 1 \wedge \forall f \in \{1,\dots,F\},\ t_{b_{f_{period}}} = T_{short} \\ T_{start_{night\_ban}} - T_{end_{night\_ban}}, & b_f > 1 \vee \exists f \in \{1,\dots,F\},\ t_{b_{f_{period}}} \geq T_{long} \end{cases}$$

If the constraint Equation 3.12 is fulfilled, the start time of the night break is the time $t_{n_{g-1}}(\widetilde{t}^{start}_{r_i(day)})$, in other words one node before the daily driving time of the fleet $t_{drive\_time_{n_g}}(day)$ has fulfilled the constraint Equation 3.12 (see Equation 3.13).

$$t_{b_f} = t_{n_{g-1}}(\widetilde{t}^{start}_{r_i(day)}), \tag{3.13}$$

$$t_{n_g}(\widetilde{t}^{start}_{r_i(day)}) > T_{start_{night\_ban}} \wedge t_{n_{g-1}}(\widetilde{t}^{start}_{r_i(day)}) \leq T_{start_{night\_ban}}$$

The length of the night break $t_{b_{f_{period}}}$ results from the end of the night driving ban $T_{end_{night\_ban}}$ minus the start of the respective break t_{b_f} (see Equation 3.14).

$$t_{b_{f_{period}}} = T_{end_{night\_ban}} - t_{b_f} \tag{3.14}$$

$$\forall\{r_1(day),\dots,r_I(day)\}\epsilon r, \forall r\epsilon R, \forall\{n()_1,\dots,n()_G\}\epsilon n,$$
$$\forall\{t_{r_1(day)},\dots,t_{r_I(day)}\}\epsilon t, \forall\{t_{b_1},\dots,t_{b_F}\}\epsilon t, \forall t\epsilon T$$

Destination

The arrival time at the destination t_{b_F}, and thus the last charging break of this fleet on this route, results from the start time of the fleet $\widetilde{t}^{start}_{r_i(day)}$ added with the total drive time of the fleet from the starting point to the destination point $t_{drive\_time_{total}}$ added with the sum of the break periods of all breaks taken by this fleet r_i (Equation 3.15).

$$t_{b_F} = \widetilde{t}^{start}_{r_i(day)} + t_{drive\_time_{total}} + \sum_{f=1}^{F-1} t_{b_{f_{period}}} \tag{3.15}$$

The length of the charging break at the destination $t_{b_{F_{period}}}$ (see Equation 3.16) is differentiated depending on the arrival time t_{b_F}. If the arrival time t_{b_F} is less than or equal to

the comparison time T_{dest}, a short charging break $T_{short_{dest}}$ is taken at the destination.

$$t_{b_{F_{period}}} = \begin{cases} T_{short_{dest}}, & t_{b_F} \leq T_{dest} \\ t_{long_{dest}}, & t_{b_F} > T_{dest} \end{cases} \tag{3.16}$$

If, on the other hand, the arrival time is greater than the comparison time T_{dest}, a long break is taken overnight. As can be seen in Equation 3.17, this long break is calculated from the end of the night break $T_{end_{night\_ban}}$ minus the arrival time at the destination t_{b_F}.

$$t_{long_{dest}} = T_{end_{night\_ban}} - t_{b_F} \tag{3.17}$$

$$\forall\{t_{b_1}, ..., t_{b_F}\} \epsilon t, \forall t \epsilon T$$

Energy demand

For each charging break b_f, the energy demand e_{bet} of the corresponding fleet $r_i(day)$, related to one BET, required since the start or since the last break (b_{f-1}) is also calculated and saved. This results from Equation 3.18. For this calculation of e_{bet}, the distance d driven by the fleet since the start of the fleet or, if $b_f \geq 1$, the distance d driven by the fleet $r_i(day)$ since the last break is multiplied by the average consumption of a BET C_{AVG} (Equation 3.18). This amount of energy corresponds to both the energy consumed by a BET before the respective charging break and the energy-charged during the respective charging break, as each BET is always fully charged to 100 % SoC in each charging break.

$$e_{bet} = d \cdot C_{AVG}, \; e_{bet} \leq C_{batt} \tag{3.18}$$

The constraint for the SoC is Equation 3.19, which specifies that the SoC may only be between 0 % and 100 %.

$$SoC = \frac{C_{batt} - e_{bet}}{C_{batt}}, \quad 0\,\% \leq SoC \leq 100\,\% \tag{3.19}$$

3.4.4 Charging flexibility

For flexibility, the minimum charging capacity required to recharge all BETs fully s at each break with the given charging time is first calculated (Equation 3.20), summed up for a time step T and a NUTS3 region. This results from the required energy e_{bet} per

BET and charging break, divided by the respective charging time of this charging break and this fraction multiplied by the number of BETs in this fleet $r_i(day)$.

$$p_{min} = \sum_{t}^{T} \sum_{n}^{N_{NUTS3}} \frac{e_{bet}}{t_{b_{f_{period}}}} \cdot r_i(day) \tag{3.20}$$

The same is done for the maximum possible charging capacity p_{max}. In Equation 3.21 p_{max} is calculated by multiplying the maximum possible charging speed of a BET by the number of BETs in this fleet $r_i(day)$ added up to a time step T and a NUTS3 region.

$$p_{max} = \sum_{t}^{T} \sum_{n}^{N_{NUTS3}} P_{max\_chargespeed} \cdot r_i(day) \tag{3.21}$$

The flexibility of the charging capacities, also referred to below as reserve power, Δp (Equation 3.22) results from the summed, maximum possible charging capacity p_{max} minus the summed, minimum required charging capacity p_{min} in order to fully recharge all BETs of the respective time step T and the respective NUTS3 region at each charging break.

$$\Delta p = p_{max} - p_{min} \tag{3.22}$$

In addition, a $P_{Limit_{min}}$ and a $P_{Limit_{max}}$ are introduced to limit the installed charging capacities. $P_{Limit_{min}}$, which is the minimum required to charge all BETs fully in the respective charging pauses in the period under consideration T_{ob} from T_{start} to T_{end}, is the p_{min} maximum of this period T_{ob} (see Equation 3.23).

$$P_{Limit_{min}} = \max_{T_{ob} \in [T_{start}, T_{end}]} p_{min,T_{ob}} \tag{3.23}$$

$P_{Limit_{max}}$, which represents the maximum possible charging capacity resulting indirectly from the maximum number of connected BETs in a time step T and NUTS3 region, is the maximum of p_{max} in the period under consideration T_{ob} (see Equation 3.24).

$$P_{Limit_{max}} = \max_{T_{ob} \in [T_{start}, T_{end}]} p_{max,T_{ob}} \tag{3.24}$$

$$\forall \{t_{b_1}, ..., t_{b_F}\} \epsilon t, \forall t \epsilon T, \forall \{r_1(day), ..., r_I(day)\} \epsilon r, \forall r \epsilon R, \forall \{n()_1, ..., n()_G\} \epsilon n$$

3.5 Model implementation

The model and the diagram representations are implemented in the IDE PyCharm [34] in the Python [35] language.

The following packages are used for this. The ast package [36] is used to ensure that the structure of the simulation code and the variables are handled efficiently for validation and debugging purposes. The Pandas library [37] is indispensable for model simulation and data processing, especially for filtering, managing, and using the large CSV-based datasets with European truck routes and corresponding traffic volumes in the simulation. The Numpy package [38] is used for efficient numerical operations and matrix-based calculations, which are of central importance for analyzing simulation results such as power reserve and charging flexibility potential. The random module [39] introduces controlled stochastic variability in the simulation, for instance, to model uncertainties in battery charging behaviors or route usage. The random module [39] generates the normally distributed start times. The datetime package [40] is crucial for processing and analyzing time-based data within the simulation model and enables precise temporal aggregation and representation of the charging flexibility potential across different regions and periods. The multiprocessing library [41] is incorporated to parallelize the simulation processes, significantly improving performance and reducing computation time. This is otherwise substantial due to the complexity of bottom-up simulations involving numerous European truck routes. The time module [42] measures execution times for model runs, ensuring the performance efficiency of the multiprocessing implementation is validated. The os package [43] facilitates file system navigation and management, enabling automated loading and saving of simulation input and output files. The matplotlib library [44] is used for generating visual representations, including bar charts and graphs, to illustrate the simulation results. The JSON module [45] enables structured storage and retrieval of input configurations and model results, ensuring reproducibility and modularity in simulation runs. Lastly, the pickle package [46] is applied to serialize and save large Python objects, such as preprocessed data or intermediate simulation results, which can be quickly reloaded to streamline iterative analyses. By combining these packages, the model efficiently simulates and calculates the charging flexibility potential and reserve power for various regions and periods.
All maps are created using the QGIS [47] software. In addition to the self-generated data from the simulation, shape data from Eurostat [48] for the representation of the NUTS3 regions and the maps from OpenStreetMap Contributors [49] are used as the data basis.

3.6 Input Data and assumptions

This section describes the input data used to simulate the model described in Section 3.2 and Section 3.3, as well as the underlying assumptions. First, the assumptions made are presented and justified in Subsection 3.6.1, then all further input data are shown

and described in Subsection 3.6.2. The year under consideration in all the following chapters is 2030, and the one-time step corresponds to 15 min.

3.6.1 Model assumptions

One of the basic assumptions is that all truck batteries are fully loaded at the start of the simulation and are also fully loaded again at every break. The legal regulations for truck drivers and journeys in Austria are assumed for all routes, including those outside Austria, to simplify the simulation. This means that a daily night-time driving ban from $T_{start_{night\_ban}} = 22{:}00$ to $T_{end_{night\_ban}} = 5{:}00$ is implemented, and possible exemptions are not taken into account.
In addition, a maximum driving time of $T_{drive\_time\_limit} = 4.5\ h$ and a maximum driving time per day of $T_{day_{max}} = 9\ h$ is assumed. The possible legal exception per truck driver of being allowed to drive 10 h a day once a week is not implemented, as the routes are implemented fleet by fleet. As the law requires, the break between the two 4.5 h blocks per day is set at $T_{short} = 0.75\ h$. If $T_{day_{max}}$ is reached, the legally prescribed long break at the end of a day is at least $T_{long} = 9\ h$ long. However, the long break period varies depending on the start time due to the night driving ban. Therefore, the basic legal requirements for a truck driver's daily driving times and the night driving ban are complied with, but no possible exceptions are considered. Special exceptions to the weekend and public holiday driving ban for trucks are included by relying on actual traffic data from ASFINAG. [33, 50]
With regard to the speed driven, the average speed of trucks on E-roads, i.e., freeways, is set at $V_{e-roads} = 80\ km/h$ and the average speed on all other roads is set at $V_{others} = 60\ km/h$. These speeds can deviate significantly from the actual average speeds due to traffic jams and the like. According to a study by Weller et al. [51], the actual usual speed of trucks on Austrian freeways is 84.7 km/h. Therefore, in Section 4.3 a consideration with increased speed ($V_{e-roads} = 87\ km/h$, $V_{others} = 67\ km/h$ - scenario higher speed), but also with lower speed ($V_{e-roads} = 70\ km/h$, $V_{others} = 50\ km/h$ - scenario lower speed), if there should be more congestion due to the higher traffic volume.
In a further study on truck speeds on Austrian freeways by Rexeis et al. [52], trucks were counted and measured at specific points on the Austrian freeways at certain times. The trucks counted at all counting locations in this study are summarized in a diagram in Figure 3.8. This shows that the first peak of trucks driving on the freeways is between 8:00 and 9:00. Based on this, the start time of the trucks is set here with an expected value $\mu = 8{:}00$ and a variance $\sigma^2 = 1\ h$.
The arrival time, which determines the length of the break on arrival at the destination, is set to $T_{dest} = 18{:}00$, since in Figure 3.8 between 17:00 - 19:00 the most significant drop in the number of trucks on the freeways is recorded, and then the number of trucks only increases again from 4:00 - 5:00.

The length of the break, which is taken at the destination before the time T_{dest}, is defined as $T_{short_{dest}} = 1\ h$. The break length, if the arrival time is after T_{dest}, is at least $T_{long_{dest}} = 7\ h$, but varies depending on the actual arrival time, which can be between 18:00 - 22:00.

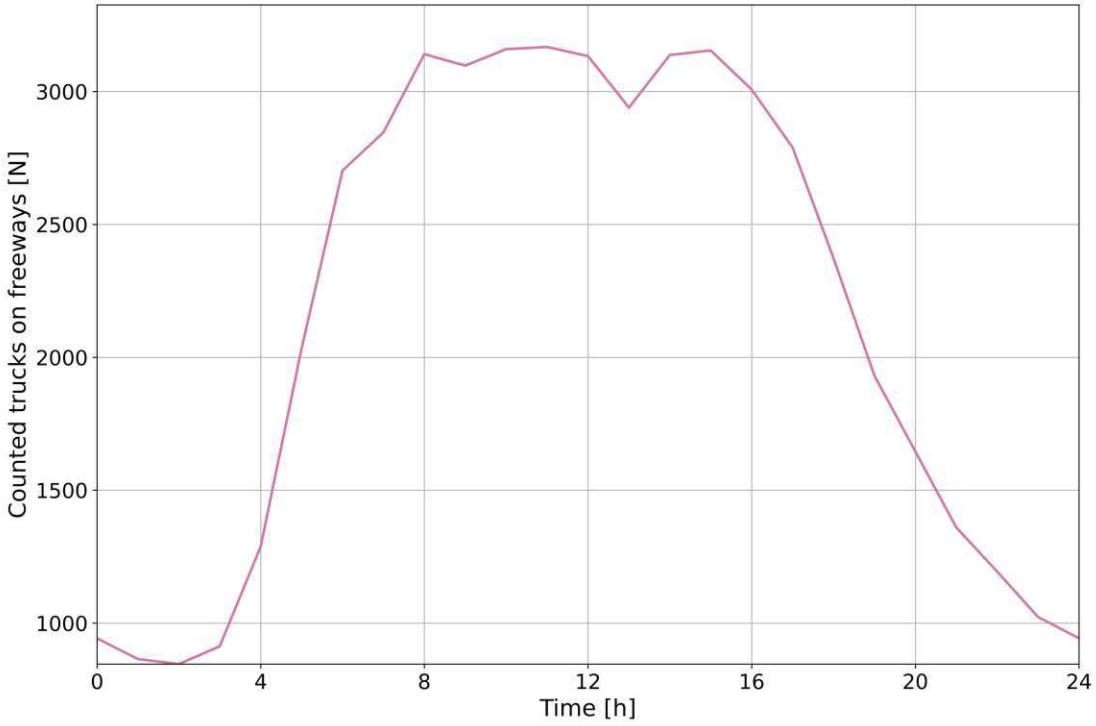

Figure 3.8: Trucks counted at certain freeway locations in Austria, based on data from KfV and ASFINAG [52]

As in the article by Speth et al. [53], the share of BETs in the total truck fleet is assumed based on the expected necessary zero-emission trucks, which were calculated from the current EU CO_2 fleet targets for trucks [54]. In this article by Speth et al., 2022, an Battery electric truck (BET) share of 15 % is assumed for HDVs in Germany. The article by Shoman et al. [55] derives an assumption of 15 % BETs in the total truck fleet for Europe. Therefore, the value $X_{BET} = 0.15$ is also set here for the proportion of BETs, as the routes are considered Europe-wide with reference to Austria (national, export, import, and transit routes).

3.6.2 Model input Data

The other model input data used are shown and referenced in the following, and the two datasets mentioned in Subsection 3.1.2 are explained in more detail.
The maximum battery capacity per truck is assumed to be $C_{Batt\_max} = 600\ kWh$, as assumed in a feasibility study by Will et al. [56] for long-haul trucks. The maximum charging speed per truck is assumed to be $P_{max\_chargespeed} = 600\ kW$ (thus 1C). This value is chosen because it is below the new, according to Heliox new universal standard [57], megawatt charging system (MCS up to 3.75 MW), but above the current combined charging system (CCS up to 375 kW) and can therefore be assumed to be realistic for the year 2030.
There are many figures for the average consumption of an BET. According to Dou et al. [58], who looked at BETs with 38 t maximum tractive force in their study, BETs need an average of around 1.6 kWh/km in summer and around 2.2 kWh/km in winter. This seasonal difference is examined in more detail in Section 4.3 with the average seasonal consumptions mentioned below regarding the resulting flexibility. Volvo states the consumption for the Volvo FH Electric (on a 343 km long test route in Germany with a speed of 80 km/h and a total load of 40 t) as 1.1 kWh/km [59]. MAN states an average consumption of 1.2 kWh/km for its BET MAN eTruck [60].
Since the routes considered, from the dataset of Speth et al. [28], are based on a lower average charge factor of 13.6 t, the average consumption of $C_{avg} = 1.2\ kWh/km$ for the annual average is assumed here. The seasonal analysis assumes that the average consumption is $C_{avg} = 1.5\ kWh/km$ in January and $C_{avg} = 1.05\ kWh/km$ in July. For the fleet calculation, $V_{limit} = 2$ is selected as the limiting parameter, and $V_{divider} = 1$ is the dividing parameter. This results in the Equation 3.2 that a fleet i can consist of the number of BETs r_i in the range $0 < r_i < 2$.
The two datasets used are described in more detail in the following two sections.

Traffic count data

First of all, the ASFINAG traffic count data [29]. These are published retrospectively as an Excel file for each month and each year and contain the following data.
As of 06.11.2024, there are 290 counting stations, for which the number of vehicles per 24 h, as well as the days counted or estimated days, are given for each vehicle class and direction of travel, broken down by day of the week (Mon-Sun, Mon - Fri, Mon, Tue-Thu, Fri, Sat, Sundays & public holidays).

European truck routes

The dataset with the synthetic European truck routes from Speth et al. [28] is based on data from the EITSplus project, based on truck traffic from 2010.
This dataset consists of four files. The first file, "01_Trucktrafficflow", contains information about the individual routes. This route information includes the individual waypoints (edges), the number of trucks on this route for 2010, 2019, and 2030, and the start and destination locations. The other files are "02_NUTS-3-Regions", with information on the NUTS3 regions contained, "03_network-nodes" with information on the nodes, which always form an edge as a pair, and "04_network_edges" with information on these edges, which represent the waypoints of the routes in the first file "01_Trucktrafficflow".
The structure of these waypoints is shown graphically in Figure 3.2 in Subsection 3.1.2 and is also explained there. A detailed dataset description can be found in the linked Data in Brief [61].

4 Results

In this chapter, the results that emerge from the simulations of the model are shown. It is structured by the order outlined in the research question and refers to Austria in 2030. The modeled charging demand curves and the resulting flexibility potential are initially classified over time and presented accordingly (Section 4.1). The spatial distribution of the flexibility potential in Austria is then described in Section 4.2. After that, the sensitivity factors will be presented in Section 4.3.

4.1 Temporal analysis of the charging demand

The simulation results for the entire year 2030 indicate that the charging demand for BET (with consideration of public holidays) is 1.23 TWh for a BET quota of 15 %. Figure 4.1 illustrates the estimated number of BETs aggregated by arrival time in 15 min time steps in an annual average week in 2030.
A distinct peak is evident at 9:00, with 31.58 % (9883931.25 trucks in total) of all trucks projected to traverse the synthesized routes in, out, and through Austria in 2030, covering distances below < 200 km. It is estimated that 43.45 % (13627853.75 trucks in total) of all trucks will travel on routes exceeding > 650 km, which necessitate two or more stops, often including a night break.
As a result, most trucks arrive at their destination between morning and midday, as seen in Figure 4.1. The pronounced peak in Figure 4.3, both for p_{min} and for p_{max}, can be attributed to the arrival times of the BET. A more detailed examination of the charging demand is provided below.

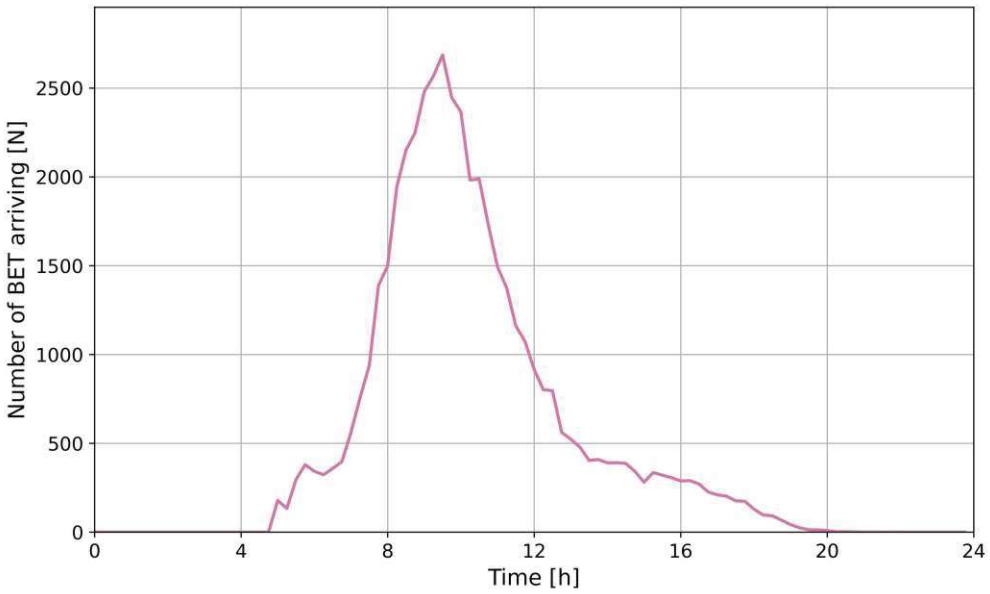

Figure 4.1: Arrival times of the trucks at the destination at an annual average week

Figure 4.2 illustrates the estimated annual average week in Austria, with an average consumption per BET of $C_{avg} = 1.2\ kW/km$ for the year 2030. The minimum developed charging capacity throughout Austria is set at $P_{Limit_{min}} = 845.41\ MW$, which corresponds to the p_{min} peak on an annual average week, which occurs on a Thursday between 10:00 - 10:15. This value should at least be reached for the installed capacities so that all BETs can be fully charged when they decide to do so according to the simulation. The maximum p_{max} for the annual average week is reached on Thursday between 9:45 - 10:00 and sets the parameter $P_{Limit_{max}} = 2040.19\ MW$ for further considerations. This value represents the maximum charging capacity required in the annual average. In general, it can be observed that there is significantly less traffic at weekends (due to the weekend driving ban in Austria), and therefore, less charging capacity is required. Sunday is, consequently, the day with the least required charging capacity. Demand rises sharply on Monday and continues to grow until the aforementioned peak on Thursday. p_{min} and p_{max} follow a recognizable daily rhythm. A peak around midday, a sharp drop until around 16:00 in the afternoon, and a relatively stable plateau in the evening and at night until both values reach their lowest point with a sharp drop at 5:00 in the morning.

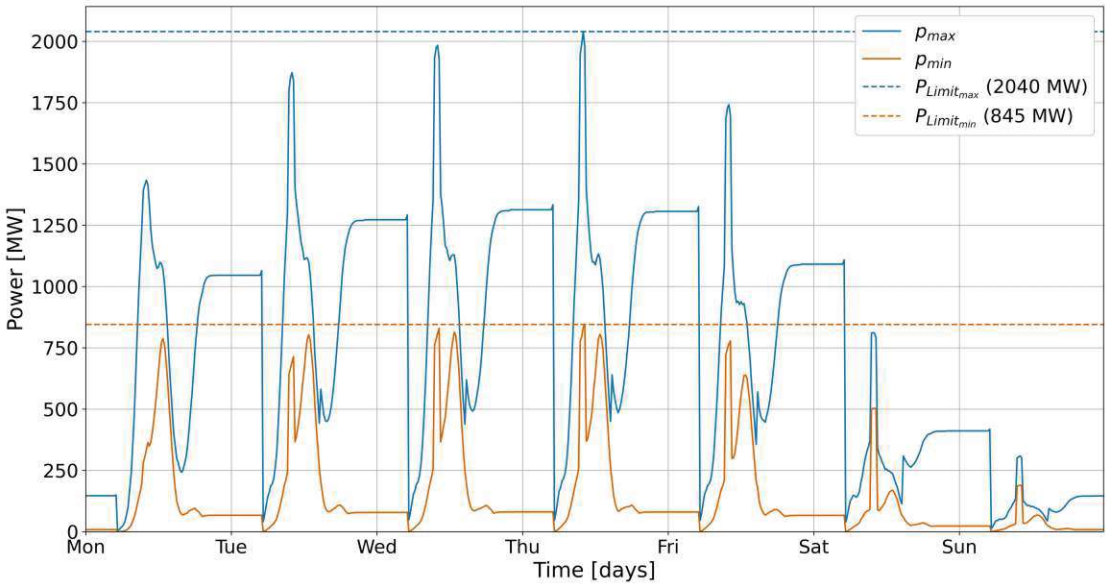

Figure 4.2: Annual charging demand summarized over the whole of Austria on an annual average

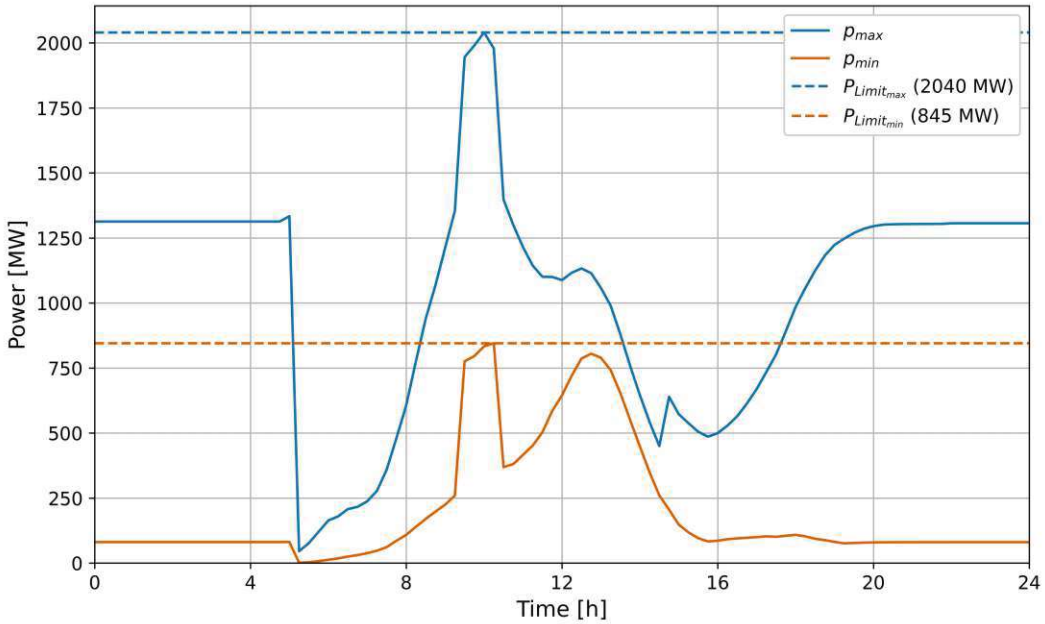

Figure 4.3: Annual charging demand summarized over the whole of Austria on an annual Thursday

Figure 4.3 illustrates the Thursday at which the maximum values $P_{Limit_{min}}$ and $P_{Limit_{max}}$ are reached in more detail. On the one hand, the stable plateau can be observed between approximately 20:00 - 5:00, and the volatile area between 5:00 - 20:00. In this volatile range, the p_{min} curve typically follows the p_{max} curve with a minor discrepancy. This is particularly evident during the pivotal period for photovoltaic (PV) in summer, between 12:00 - 14:00, when the sun is at its highest point. The P_{Limit} and thus the actually installed capacities are decisive, especially for the usable flexibility during the day, as to whether any or sufficient flexibility is available.
Between 18:00 - 5:00, on the other hand, stable flexibility can be expected according to the figure. This can be useful for wind power in the winter months.
To get an overview of winter to summer comparison, in Figure 4.4, an average consumption of $C_{avg} = 1.05\ kW/km$ is assumed for July and $C_{avg} = 1.5\ kW/km$ for January (see Section 3.6 why additional consumption is assumed in January/winter). For both months, a Thursday of an average week of the respective month is selected for closer examination. The individual curves are almost identical, but the dashed p_{min} curve for January rises faster, especially during the volatile time of day between 5:00 - 13:00. This reduces the usable flexibility at the corresponding times. Depending on the installed charging capacities, this can also result in the charging demand not being fully met. At night, this effect is only minor. These two months hardly make any difference in the number of trucks on the road, and they must take breaks. This can be seen above all in the almost identical p_{max} curves. The increased p_{min} curve in January compared to July is due to the assumed increased consumption, as the BETs then require more energy during the same break time.

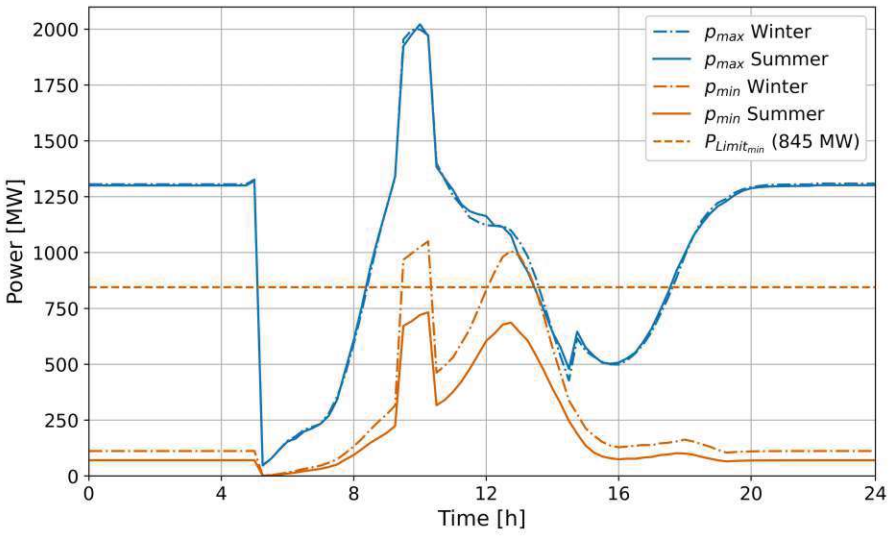

Figure 4.4: Seasonal comparison of charging demand in January and July

4.2 Spatial analysis of the charging demand

The spatial distribution of the flexibility potential is analyzed for the illustrations with a limitation of the installed capacities P_{Limit}. This allows a limited maximum of installed charging capacities, specific to each NUTS3 region in Austria, to be included in the analysis. A value of $P_{Limit_{min}} = 845.41\ MW$, summed across all NUTS3 regions in Austria, is selected as the maximum. This value corresponds to the p_{min} maximum on an annual average Thursday for all NUTS3 regions in Austria. Broken down to the individual NUTS3 regions, this means that in the plots with a limit, the P_{Limit} is the p_{min} maximum of the respective NUTS3 region within the annual average Thursday. The illustrations are selected for different time frames that stand out specially in the temporal illustrations. At the end of the Subsection 4.2.1, there is also a spatial representation, which shows the expected reserve capacity value of a 15 *min* time step averaged over a year for each NUTS3 region in Austria. The selected time frames are always 15 *min* long. These time frames, considered in more detail below, are colored in Figure 4.5 for an annual average Thursday, as previously shown, and are defined in Table 4.1.

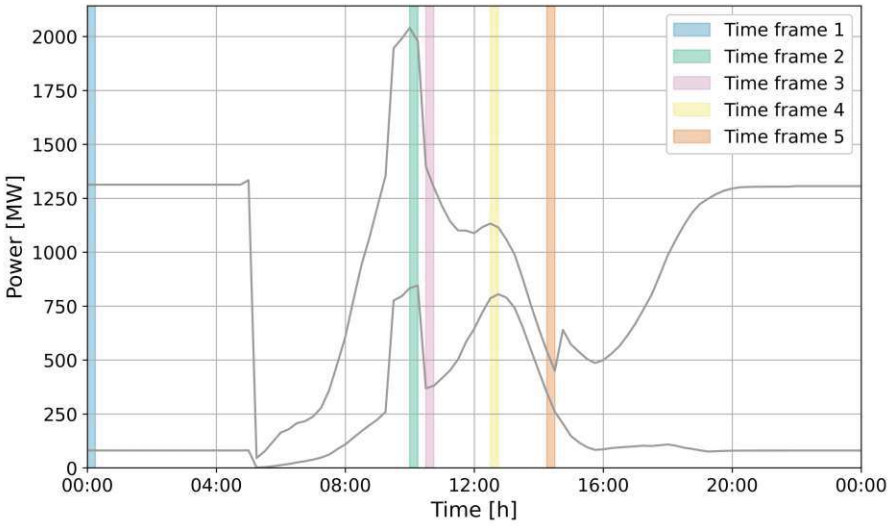

Figure 4.5: Time frames analyzed in terms of spatial distribution

The time frame 1 from 00:00 - 00:15 is chosen to show the spatial distribution on the stable plateau at night, which is interesting for reserve power, for example, when it comes to wind energy. The spatial distribution at night is static in the model, as the implemented night-time driving ban means that the BETs are permanently connected

to one location without changing location during this time. In addition to this nighttime analysis, several midday time frames are examined, as they are also significant for reserve power, particularly concerning PVs. These midday time frames are as follows. Time frame 2 from 10:00 - 10:15 where the maximum of p_{min} is. Then the time frame 3 from 10:30 - 10:45 where the p_{min} curve has dropped significantly before it peaks again in time frame 4 from 12:30 - 12:45. Time frame 5 from 14:15 - 14:30 is selected because the afternoon minimum of p_{max} is located during this time.

Time [h]	Time frame number
00:00 - 00:15	1
10:00 - 10:15	2
10:30 - 10:45	3
12:30 - 12:45	4
14:15 - 14:30	5

Table 4.1: Time frame times

The time frames are evaluated with the available reserve power $\Delta p = p_{max} - p_{min}$ on an annual basis ($C_{avg} = 1.2\ kW/km$). As $P_{Limit_{min}}$ is included in the calculation for the illustrations in Subsection 4.2.1 with a limit as p_{min} maximum over an annual week, Δp can be a minimum of zero. In Subsection 4.2.2, this analysis is repeated with a $P_{limit_{max}}$ (which corresponds to a limit at the maximum of p_{max}, which corresponds to an installed capacity without limit) for selected time frames in order to have a comparison of the extent to which the spatial distribution of the reserve power would change if there were no limitation of the installed capacities. The coloring of the scale is based on the following assignments: Red stands for a small to zero reserve power Δp, white for the medium transition range, and blue for a large Δp. First, in Subsection 4.2.1, the spatial distribution of flexibility with $P_{Limit_{min}}$ is shown, followed by a comparison for selected time frames with $P_{Limit_{max}}$ in Subsection 4.2.2.
The following two figures and two tables show the number of BETs plugged in over a specific time frame to illustrate HDVs traffic in Austria. Figure 4.6 and Table 4.2 show the spatial distribution for all NUTS3 regions in Austria and the corresponding values for the NUTS3 regions with the ten highest numbers of plugged-in BETs for time frame 1 (from 00:00 - 00:15). In Figure 4.7 and Table 4.3, this can be seen for time frame 2 (from 10:00 - 10:15). During the night, represented by time frame 1, 2188.52 BETs are plugged in for charging in Austria. Many of them are plugged in in the regions in Upper and Lower Austria (Table 4.2). Styria and Carinthia have isolated regions with more than 77 of plugged-in BETs (Graz and Lower Carinthia, respectively). In Vorarlberg, Tyrol, and parts of Burgenland (especially southern and central Burgenland), on the other hand, only a few BETs are plugged in over a large area. In time frame 2, a maximum of

3400.31 BETs are plugged in. Again, these are mainly plugged in in Upper and Lower Austria. But now also more in the regions of Styria, Salzburg and surroundings as well as in Carinthia (Figure 4.7). In the western regions, such as Vorarlberg and Tyrol, but also parts of Burgenland (especially southern and central Burgenland), the plugged-in BETs have not increased or decreased significantly and remain at a low level. However, the number of BETs plugged in does not necessarily equate directly to the available flexibility potential. This is illustrated in the following sections.

NUTS3 region	plugged-in BETs $[N]$
Linz-Wels	270.22
Innviertel	252.04
Mostviertel-Eisenwurzen	196.52
Steyr-Kirchdorf	148.31
Vienna environs southern part	136.81
Eastern Styria	126.93
Klagenfurt-Villach	109.79
Graz	87.77
Lower Carinthia	77.01
St. Pölten	74.00
Austria in total	2188.52

Table 4.2: Top 10 NUTS3 region with the highest number of BETs plugged-in during time frame 1 from 00:00 - 00:15

NUTS3 region	plugged-in BETs $[N]$
Vienna	286.84
Vienna environs southern part	280.35
Linz-Wels	241.00
Mostviertel-Eisenwurzen	230.54
Innviertel	188.50
Graz	151.28
Vienna environs northern part	150.70
Liezen	127.47
Salzburg and surroundings	123.49
St. Pölten	120.79
Austria in total	3400.31

Table 4.3: Top 10 NUTS3 region with the highest number of BETs plugged-in during time frame 2 from 10:00 - 10:15

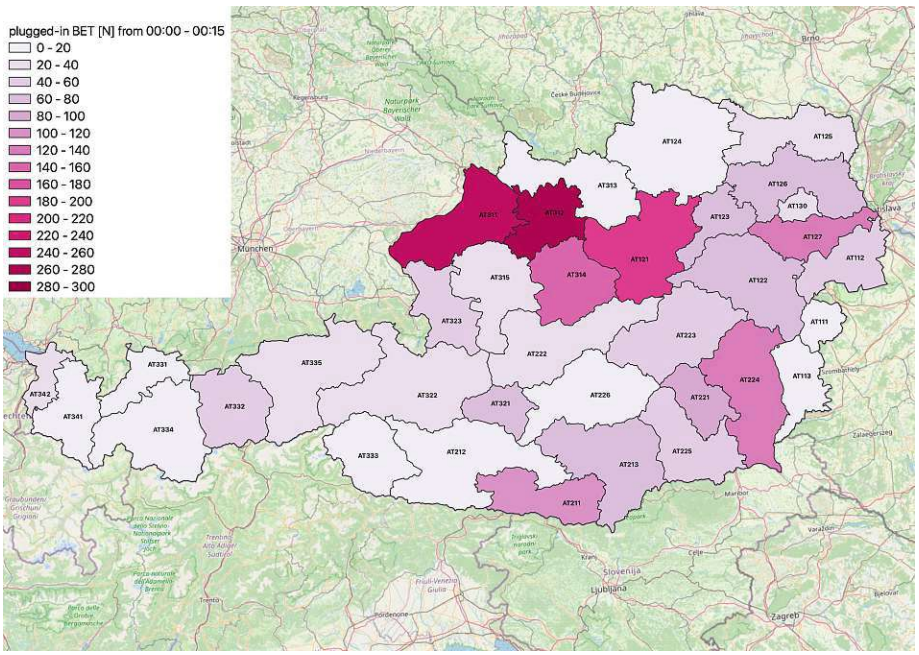

Figure 4.6: Number of BETs plugged-in per NUTS3 region in time frame 1 from 00:00 - 00:15

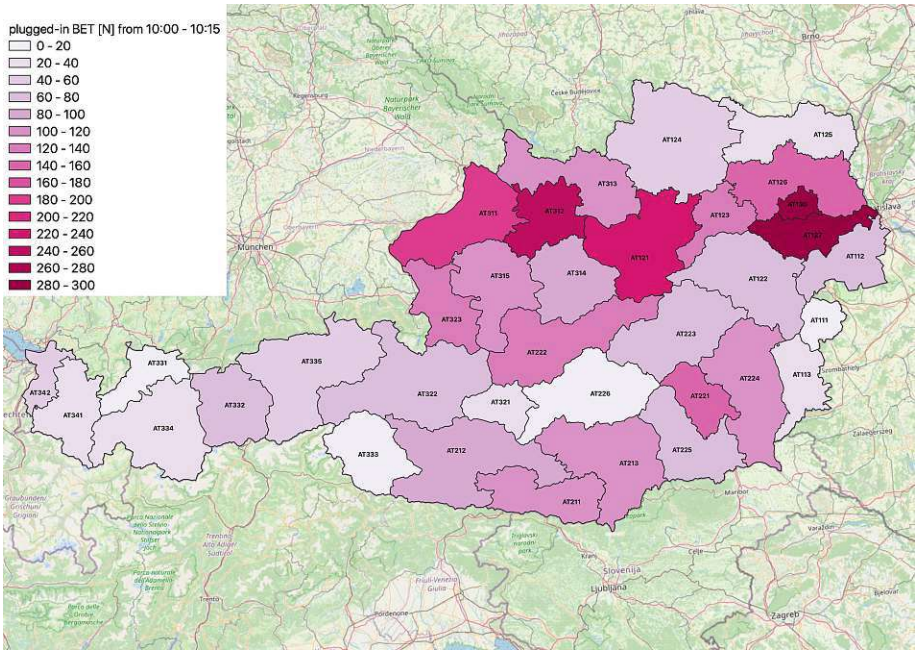

Figure 4.7: Number of BETs plugged-in per NUTS3 region in time frame 2 from 10:00 - 10:15

4.2.1 Spatial analysis with limit

Figure 4.8 shows Austria divided into NUTS3 regions in the time frame 1 from 00:00 - 00:15, colored for the corresponding reserve power Δp values.
The regions Linz-Wels with 83.36 MW and western upper Styria with 0 MW stand out in the upper and lower Δp range (see Table 4.4). In Linz-Wels, 270.22 BETs are plugged in with a maximum available charging capacity of 346.51 kW per BET. The high Δp is created by the long time that these are plugged in, so a single BET has a very small p_{min} of 38 kW per BET, which is sufficient to charge it during the specified night break entirely.
A wide range of Δp values can generally be observed due to the long break time/night driving ban. This spatial distribution is stable during the night driving ban period (from 22:00 - 05:00) (compare with Figure 4.3).

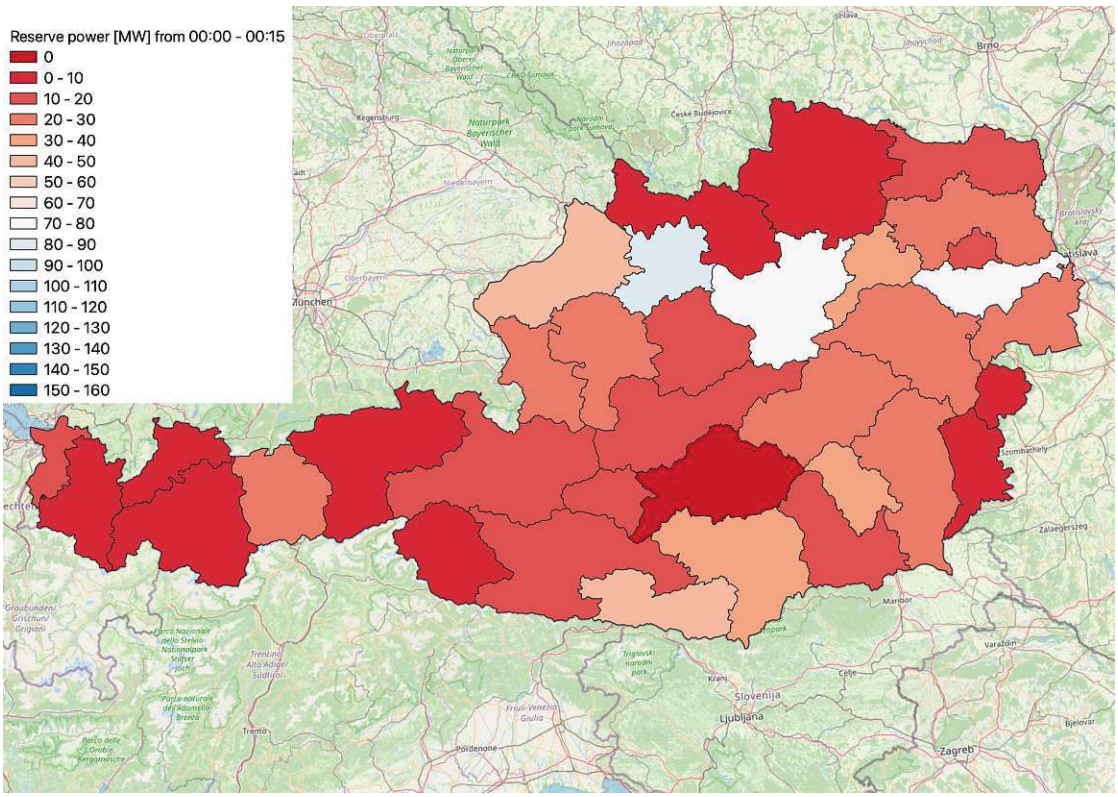

Figure 4.8: Spatial distribution of reserve power from 00:00 - 00:15 with limited installed charging capacity

NUTS3 region	Δp $[MW]$	plugged-in BETs $[N]$
Linz-Wels	83.36	270.22
Vienna environs southern part	76.93	136.81
Mostviertel-Eisenwurzen	75.78	196.52
Außerfern	0.46	0.81
Central Burgenland	0.04	0.07
Western upper Styria	0.00	0
Austria in total	798.20	2188.52

Table 4.4: Highest and lowest Δp values from 00:00 - 00:15 with limited installed charging capacity

As illustrated in Figure 4.9, the time frame 2 between 10:00 - 10:15 is worthy of particular attention. During the aforementioned period, 27 of the 35 regions exhibited a power output between 0 MW and 9.31 MW. Five regions are between 13.52 MW to 18.54 MW, and the remaining three regions are between 25.34 MW to 52.20 MW.
The range of the Δp value (Table 4.5) is markedly smaller than that observed during the night hours, with most values falling within the low range, as evidenced by the red coloring. The regions of Linz-Wels are particularly interesting with a Δp of 52.20 MW and the southern environs of Vienna with 0 MW. In Linz-Wels, there are now 241.00 plugged-in BETs with a maximum available charging capacity of 388.52 MW per BET. Due to the significantly shorter charging times for some BETs, but less available charging power Δp than at night in time frame 1. With 280.35 plugged-in BETs and 296.42 MW per BET charging capacity, the southern environs of Vienna have less available charging capacity per BET than Linz-Wels. However, the $\Delta p = 0$ MW is mainly because the $P_{Limit_{min}}$, and thus the installed capacities, are completely exhausted in this region in time frame 2.

NUTS3 region	Δp $[MW]$	plugged-in BETs $[N]$
Linz-Wels	52.20	241.00
Innsbruck	25.58	69.73
Salzburg and surroundings	25.34	123.49
Mühlviertel	0.0	106.01
Steyr-Kirchdorf	0.0	93.13
Vienna environs southern part	0.0	280.35
Austria in total	233.59	3400.31

Table 4.5: Highest and lowest Δp values from 10:00 - 10:15 with limited installed charging capacity

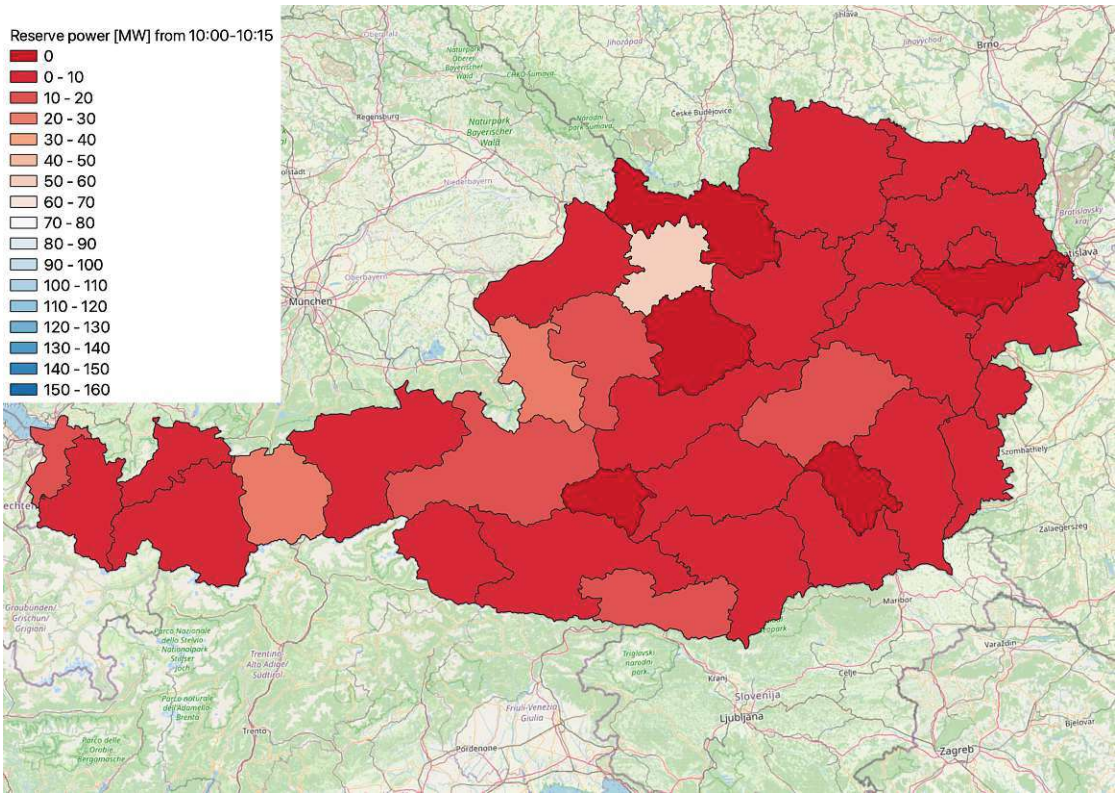

Figure 4.9: Spatial distribution of reserve power from 10:00 - 10:15 with limited installed charging capacity

Figure 4.10 shows that the Δp in the time frame 3 from 10:30 - 10:45, after the Austria-wide p_{min} maximum (=$P_{Limit_{min}}$) in the time frame 2 (see Figure 4.5), rises to a higher level in many NUTS3 regions when the $P_{Limit_{min}}$ is included in the analysis.
In contrast to the previous time frame, a shift in the spatial distribution can be seen. The highest value for Δp is no longer measured in Linz-Wels southern, but in the southern environs of Vienna with 63.36 MW (Table 4.6). The two regions with the most reserve power compared individually are Linz-Wels with $+5.59$ MW, but the southern environs of Vienna with $+63.36$ MW, as in the previous time frame 2, this region reached its $P_{Limit_{min}}$ and thus all the installed capacities assumed in the simulation were in use. In contrast, fewer BETs (146.75) are plugged in in time frame 3, and a maximum of 566.28 kW charging power per BET is available. As this is not fully required to charge the BETs in their specified break time (p_{min} per BET is also much lower in this time frame 3 than in the previously considered one (p_{min} per BET $= 134.49$ kW in time frame 3 versus p_{min} per BET $= 296.42$ kW in time frame 2) and substantially more available installed capacities are available, significantly more reserve power is available.

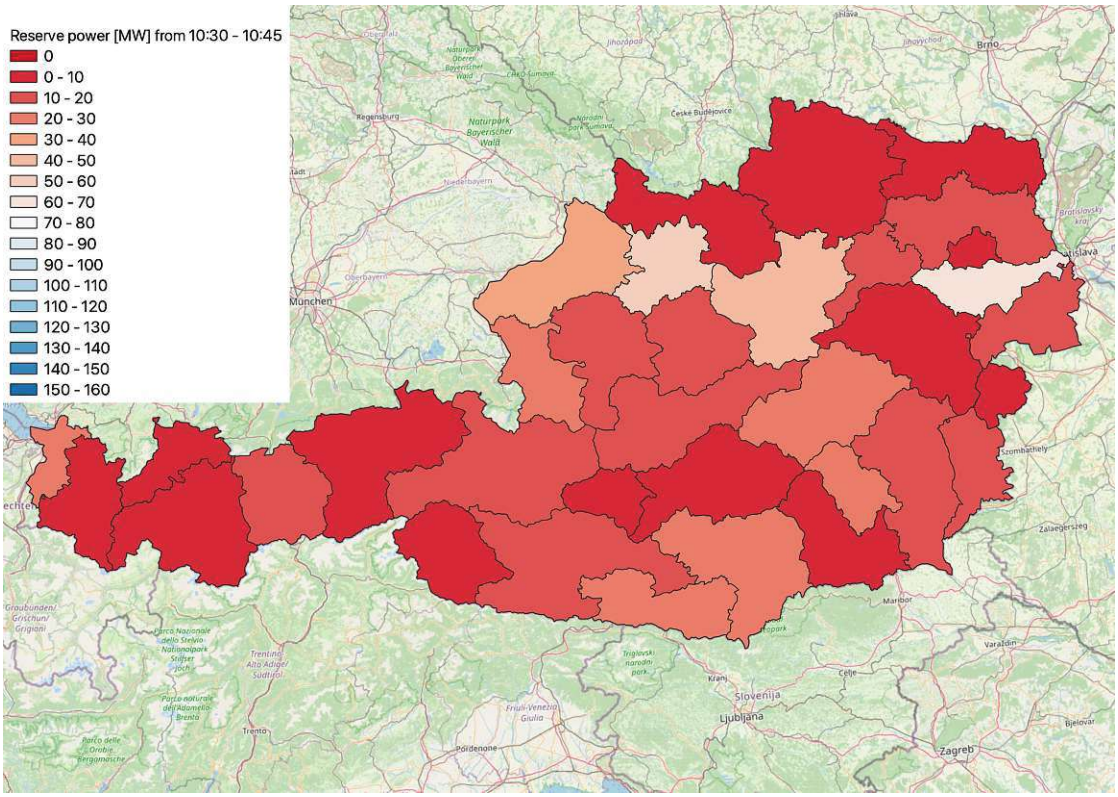

Figure 4.10: Spatial distribution of reserve power from 10:30 - 10:45 with limited installed charging capacity

NUTS3 region	Δp $[MW]$	plugged-in BETs $[N]$
Vienna environs southern part	63.36	146.75
Linz-Wels	57.79	232.70
Mostviertel-Eisenwurzen	45.32	110.20
Central Burgenland	2.03	4.35
East Tyrol	1.18	3.58
Außerfern	0.17	3.49
Austria in total	583.02	2329.32

Table 4.6: Highest and lowest Δp values from 10:30 - 10:45 with limited installed charging capacity

During the midday time frame 4 (12:30 - 12:45), the Δp values remain relatively low. Nevertheless, in some eastern regions of Austria, particularly in areas traversed by the

A1 freeway (Mostviertel-Eisenwurzen and St. Pölten), as well as the southern environs of Vienna and Graz, Δp values over 11.41 MW are observed. Figure 4.11 illustrates that there are 31 of the 35 regions are situated entirely within a value range $\leq$ 8.32 MW. Compared to the preceding time frames, the entire range of Δp values has diminished once more. The highest value observed in the region southern environs of Vienna is now 18.11 MW (Table 4.7).

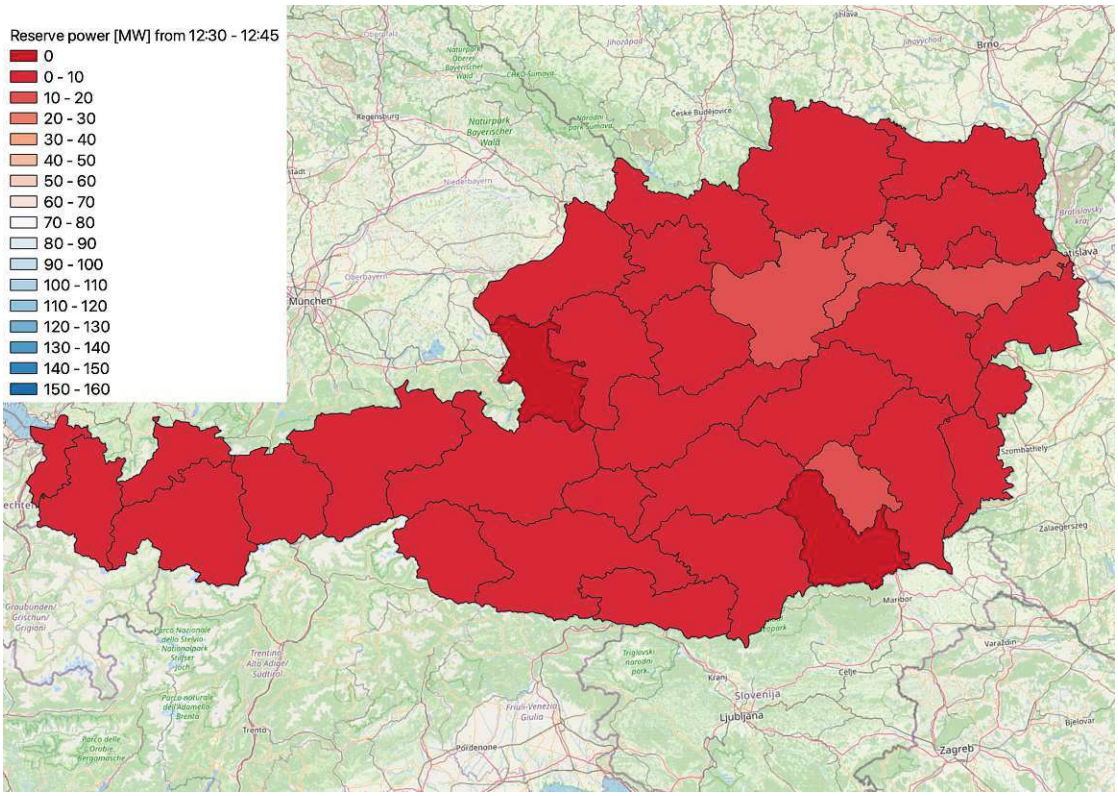

Figure 4.11: Spatial distribution of reserve power from 12:30 - 12:45 with limited installed charging capacity

NUTS3 region	Δp $[MW]$	plugged-in BETs $[N]$
Vienna environs southern part	18.11	78.48
Mostviertel-Eisenwurzen	17.01	104.42
Graz	16.16	51.39
Klagenfurt-Villach	0.34	107.48
Western and southern Styria	0.0	43.59
Salzburg and surroundings	0.0	126.21
Austria in total	147.30	1888.25

Table 4.7: Highest and lowest Δp values from 12:30 - 12:45 with limited installed charging capacity

The value range of Δp is observed to be slightly higher during the afternoon hours than to midday, in the time frame 5 from 14:15 - 14:30 (see Figure 4.12 and Table 4.8). The map is still predominantly red, indicating that most regions have a value below $10MW$ (29 of 35 regions are ≤ 7.05 MW). The highest recorded value is in the Salzburg and surroundings region, at 22.44 MW. The main reason for this is not the limitation of the installed capacities but the low number of connected BETs in combination with high p_{min} per BET values, as much energy has to be charged in short charging breaks. From this fifth time frame, the reserve power Δp in most regions (especially the regions Linz-Wels, Mostviertel-Eisenwurzen crossed by the A1 freeway, as well as the southern environs of Vienna and Innviertel) increases slowly until 16:00, then more rapidly until it reaches the high night-time plateau again from 20:00 (compare with the curves in Figure 4.5 and the spatial distribution in Figure 4.8).

NUTS3 region	Δp $[MW]$	plugged-in BETs $[N]$
Salzburg and surroundings	22.44	66.97
Linz-Wels	20.13	103.10
Innviertel	14.52	65.22
Central Burgenland	0.80	3.19
Tyrolean Oberland	0.67	5.53
Außerfern	0.53	1.49
Austria in total	185.17	904.22

Table 4.8: Highest and lowest Δp values from 14:15 - 14:30 with limited installed charging capacity

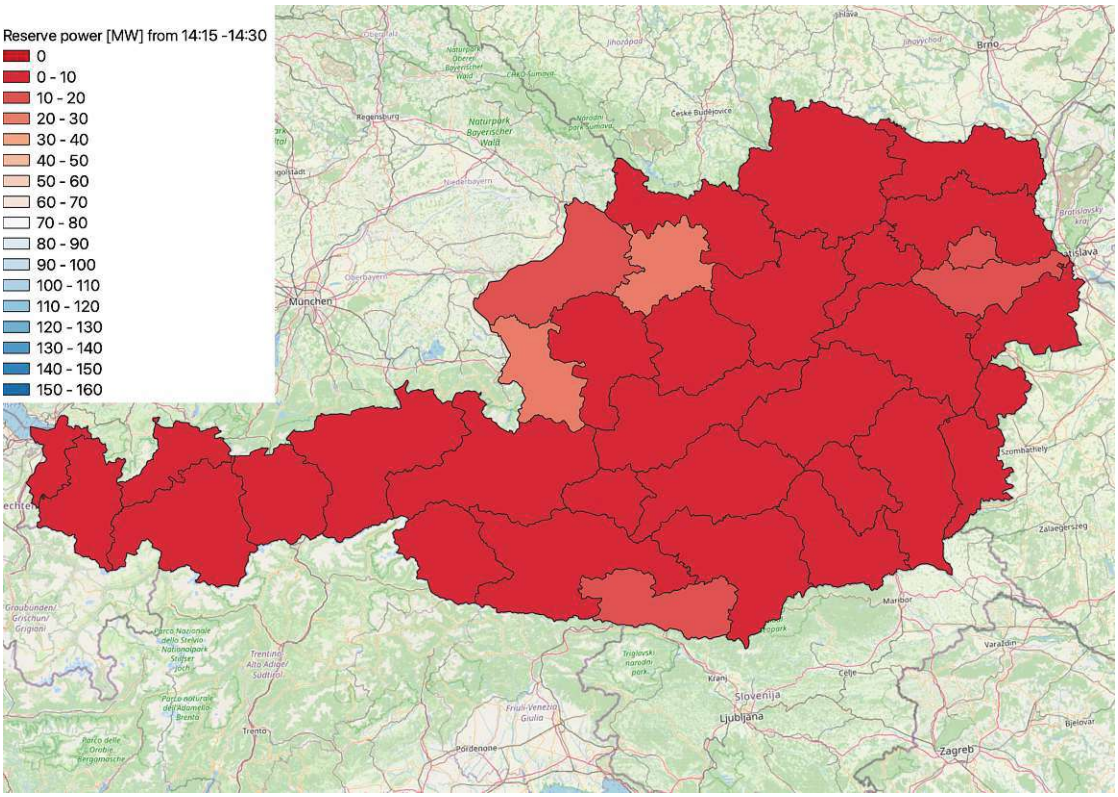

Figure 4.12: Spatial distribution of reserve power from 14:15 - 14:30 with limited installed charging capacity

The following Figure 4.13 and Table 4.9 represent the reserve power averaged over the entire year 2030 (including public holidays) for a 15 *min* time step in the respective NUTS3 region.
The three regions, Linz-Wels, Mostviertel-Eisenwurzen, and the southern environs of Vienna, clearly set themselves apart from the other regions. Here, a relatively high reserve power of over 34 *MW* can be expected on average in a 15 *min* time step in the year 2030.
The Vorarlberg region, on the other hand, stands out with a low reserve power. The same applies to large parts of Tyrol (except Innsbruck), the northern part of Upper and Lower Austria, Burgenland, the western and southern parts of Styria, the southern parts of Salzburg and the surrounding area, as well as the western part of Carinthia.

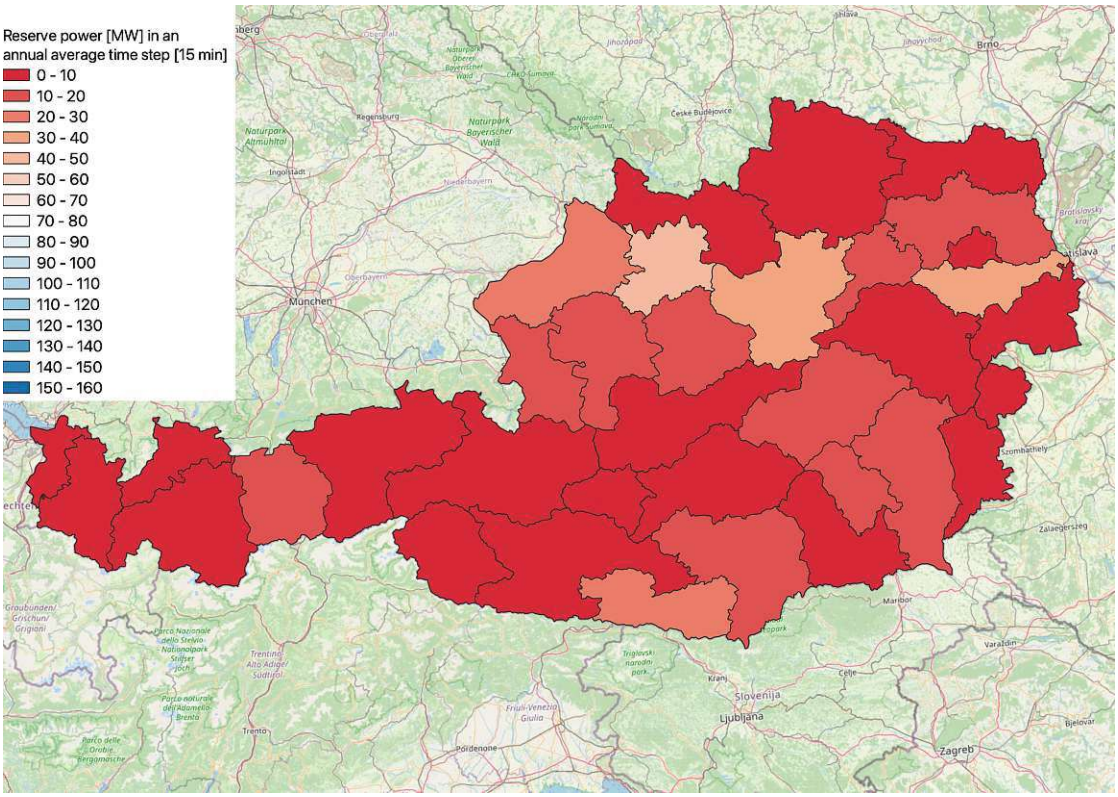

Figure 4.13: Spatial distribution of reserve power averaged over the year, for a 15 *min* time step, with limited installed capacities

NUTS3 region	Δp $[MW]$	plugged-in BETs $[N]$
Linz-Wels	45.80	137.59
Mostviertel-Eisenwurzen	36.79	90.10
Vienna environs southern part	34.73	75.16
Innviertel	27.41	110.07
Klagenfurt-Villach	23.49	57.07
Graz	18.24	46.18
St. Pölten	15.84	38.04
Salzburg and surroundings	14.99	39.11
Lower Carinthia	14.18	36.26
Innsbruck	13.68	31.59
Vienna environs northern part	13.06	46.53
Eastern Upper Styria	12.30	28.17
East Styria	12.22	55.35
Steyr-Kirchdorf	11.37	68.28
Traunviertel	11.03	27.25
Northern Burgenland	10	24.54
Lower Austria-South	9.58	31.14
Pinzgau-Pongau	9.07	21.53
Rhine Valley-Lake Constance region	8.94	21.23
Vienna	8.81	46.62
Lungau	8.64	30.85
Western and southern Styria	8.60	26.85
Liezen	7.95	20.11
Weinviertel	7.16	16.96
Upper Carinthia	5.11	12.49
Tyrolean lowlands	4.82	16.72
Mühlviertel	3.90	15.18
Southern Burgenland	3.75	9.49
Bludenz-Bregenzer Wald	2.73	7.89
Tyrolean Oberland	2.63	6.42
Waldviertel	2.61	8.31
East Tyrol	0.61	1.81
Western upper Styria	0.58	2.20
Außerfern	0.35	0.98
Central Burgenland	0.29	1.02
Austria in total	411.26	1209.09

Table 4.9: Reserve power and plugged-in BETs averaged over the year, for a 15 *min* time step, with limited installed capacities

4.2.2 Spatial analysis without limit

The following four figures (Figure 4.14, Figure 4.15, Figure 4.16 and Figure 4.17) illustrate the spatial distribution and the corresponding Δp values without any limitation by $P_{Limit_{min}} = 845.41\ MW$, but a limit of the installed capacities Austria-wide at $P_{Limit_{max}} = 2040.19\ MW$, which in real terms does not correspond to a limit of the installed capacities, as this corresponds to the maximum possible charging energy within a 15 *min* time step of an annual average week (see Figure 4.2). These figures illustrate the spatial distribution of reserve powers if the installed charging capacities were to cover all charges at the maximum charging speed.
As anticipated, elevated Δp values are evident throughout the night in the time frame 1 from 00:00 - 00:15 (Figure 4.14, Table 4.10), however, only for less than half of the regions. 20 of the 35 regions have no change in reserve power in time frame 1, with no limit on installed capacity. The regions AT111, AT113, AT124, AT125, AT127, AT130, AT212, AT222, AT223, AT226, AT313, AT315, AT322, AT323, AT331, AT332, AT333, AT334, AT341, AT342 have not changed (see Figure 3.1, Table A1 and Table A2).
There are major changes in the top three from Table 4.10. In the Mostviertel-Eisenwurzen region, reserve power increases by +46.2 %, Linz-Wels by +82.2 %, and the Innviertel by +187.9 %. In time frame 2 from 10:00 - 10:15, when the $P_{limit_{min}}$ is reached throughout Austria (Figure 4.3), the greatest changes can be seen overall (Figure 4.15, Table 4.11). In only three of the 35 NUTS3 regions is there no increase in reserve power (AT125, AT226, AT333 (Figure 3.1, Table A1 and Table A2)).
The highest reserve power values are achieved in Vienna (+183.5 %), Linz-Wels (+97.6 %), and the southern environs of Vienna (from 0.00 *MW* to 85.11 *MW*) (Table 4.11). In time frame 3 (10:30 - 10:45 see Figure 4.16 and Table 4.12) and time frame 4 (12:30 - 12:45 see Figure 4.17 and Table 4.7) the changes continue to decrease until in time frame 5 (14:15 - 14:30) there are only small changes in three regions (Table 4.14). However, for the most part, the values remain the same.

NUTS3 region	Δp $[MW]$	plugged-in BETs $[N]$
Linz-Wels	151.86	270.22
Innviertel	141.70	252.04
Mostviertel-Eisenwurzen	110.78	196.52
Außerfern	0.46	0.81
Central Burgenland	0.04	0.07
Western upper Styria	0.00	0
Austria in total	1232.31	2188.52

Table 4.10: Highest and lowest Δp values from 00:00 - 00:15 without limited installed charging capacity

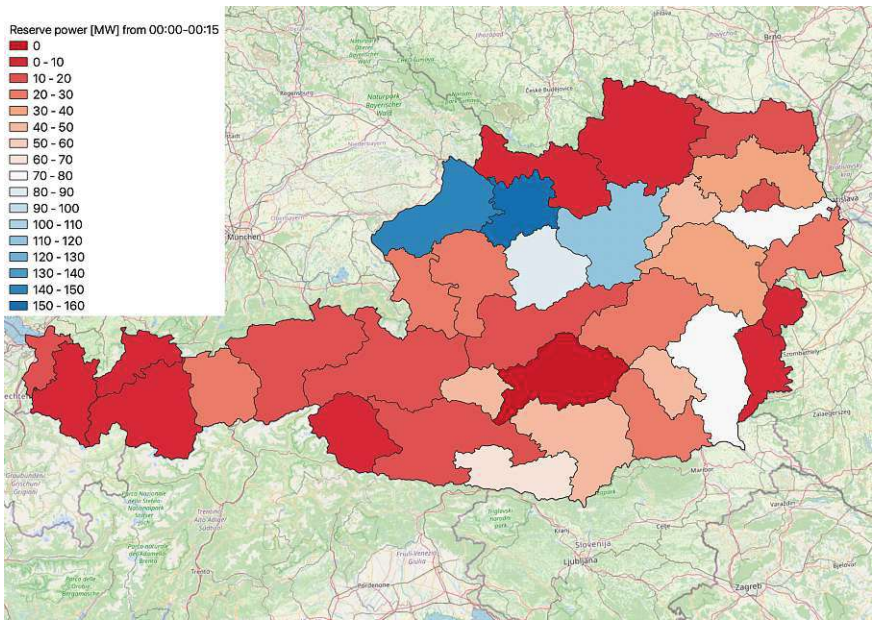

Figure 4.14: Spatial distribution of reserve power from 00:00 - 00:15 without limited installed charging capacity

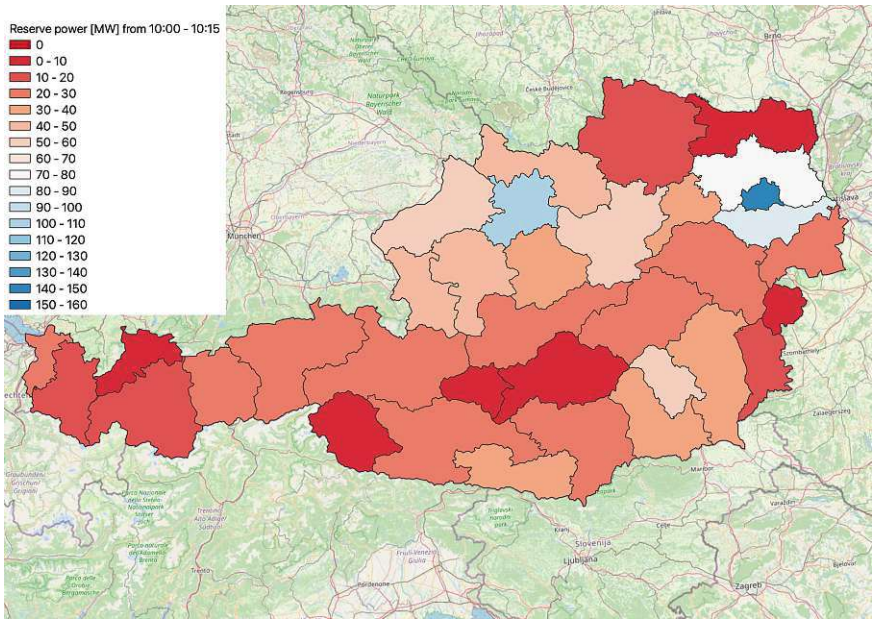

Figure 4.15: Spatial distribution of reserve power from 10:00 - 10:15 without limited installed charging capacity

NUTS3 region	Δp $[MW]$	plugged-in BETs $[N]$
Vienna	144.60	286.84
Linz-Wels	103.17	241.00
Vienna environs southern part	85.11	280.35
Central Burgenland	2.06	5.28
Außerfern	1.42	3.69
East Tyrol	0.97	3.05
Austria in total	1206.66	3400.31

Table 4.11: Highest and lowest Δp values from 10:00 - 10:15 without limited installed charging capacity

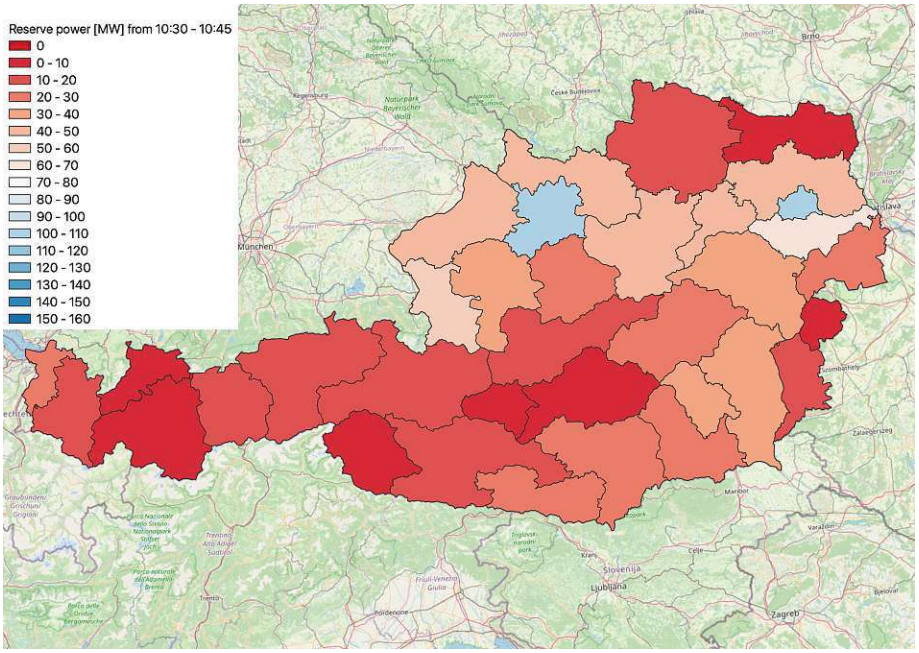

Figure 4.16: Spatial distribution of reserve power from 10:30 - 10:45 without limited installed charging capacity

NUTS3 region	Δp $[MW]$	plugged-in BETs $[N]$
Linz-Wels	103.78	232.70
Vienna	101.24	205.74
Vienna environs southern part	68.31	146.75
Central Burgenland	2.03	4.35
Außerfern	1.40	3.49
East Tyrol	1.18	3.58
Austria in total	1028.58	2329.32

Table 4.12: Highest and lowest Δp values from 10:30 - 10:45 without limited installed charging capacity

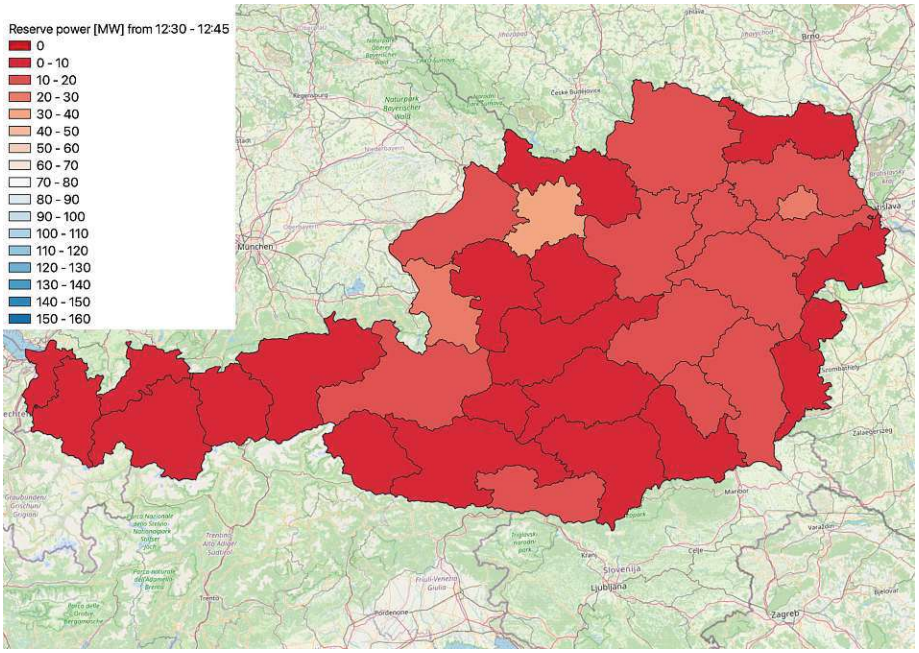

Figure 4.17: Spatial distribution of reserve power from 12:30 - 12:45 without limited installed charging capacity

NUTS3 region	Δp $[MW]$	plugged-in BETs $[N]$
Linz-Wels	34.47	205.90
Salzburg and surroundings	25.72	126.21
Vienna	24.73	83.24
East Tyrol	1.51	5.06
Central Burgenland	0.59	2.23
Außerfern	0.54	1.75
Austria in total	346.35	1888.25

Table 4.13: Highest and lowest Δp values from 12:30 - 12:45 without limited installed charging capacity

NUTS3 region	Δp $[MW]$ with $P_{Limit_{min}}$	Δp $[MW]$ with $P_{Limit_{max}}$
Tyrolean Unterland	2.06	8.31
East Tyrol	1.39	3.19
Außerfern	0.53	0.57
Austria in total	185.17	193.26

Table 4.14: Δp value changes in the time frame 5 from 14:15 - 14:30 between with and without limited installed charging capacity

4.3 Sensitivity analysis of the simulation

In the following sensitivity analysis of the simulation, the BET share (Subsection 4.3.1), the average speeds (Subsection 4.3.2) and the limitation of installed capacities P_{Limit} (Subsection 4.3.3) are considered by varying the respective values.

4.3.1 BET share

In Figure 4.18, the BET share of 15 % ($X_{BET} = 0.15$) utilized in the preceding results is contrasted with a BET share of 30 % ($X_{BET} = 0.30$). A twofold increase in the value for leads results in a twofold increase in both the values for p_{max} and for p_{min} (and consequently also the reserve powers Δp), which causes a shift of the curves on the Y-axis. The slight fluctuations and differences are due to the methodology, which employs normally distributed departure times, and the two independent simulations for this diagram.

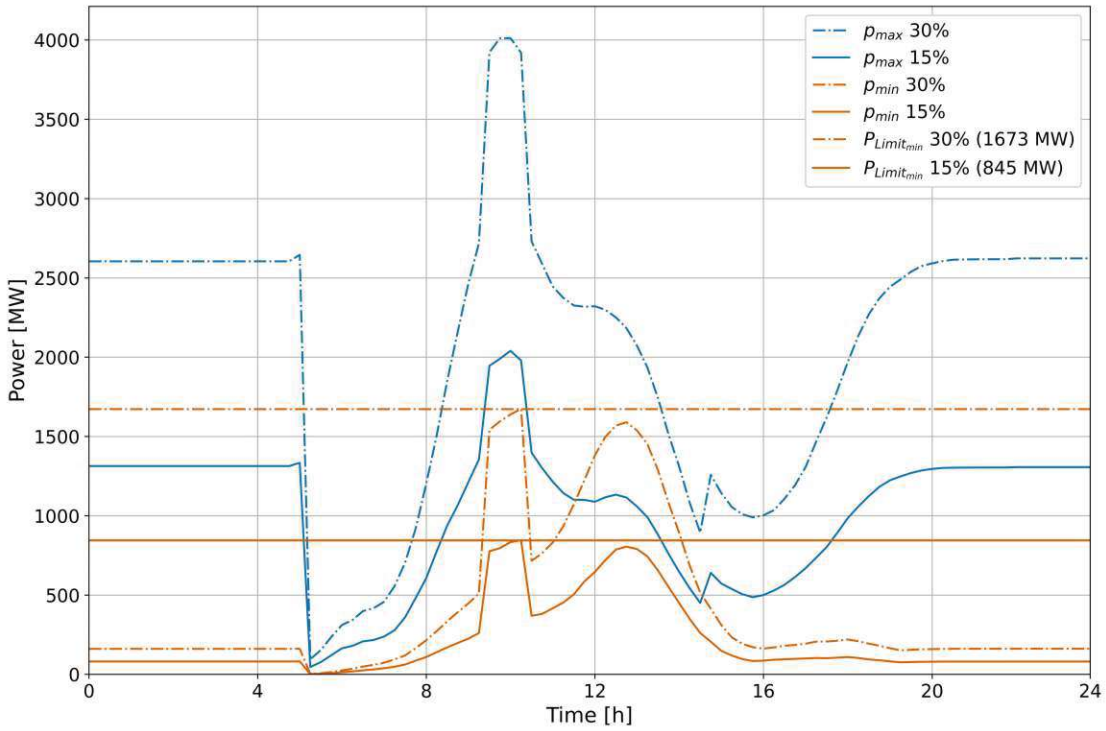

Figure 4.18: Scenario comparison of 15 % vs. 30 % BET share

4.3.2 Average speeds

The sensitivity of the average speeds is evaluated through a comparative analysis of two further scenarios to the scenario presented in the results. In the first scenario, a lower speed is assumed, while in the second, a higher speed is considered than in the results previously evaluated (previously the standard speed: 80 km/h and 60 km/h). The first scenario entails trucks driving at an average speed of 70 km/h on the E-roads and 50 km/h on all other roads.
In the second scenario, the trucks are driven at 87 km/h on the E-roads and 67 km/h on all other roads. A comparison of the results from these two simulations over time can be seen in Figure 4.20.
It can be observed that the more frequent breaks, which are required at the slower speeds (first scenario with lower speed) on a route, result in a shift in the maxima of p_{max} and p_{min} in particular (around time frame 2 from 10:00 - 10:15). Furthermore, it can be observed that the high plateau of p_{max} is also shifted upwards at night. Apart from

the increased p_{min} maximum around 10:00, the p_{min} curve does not change significantly, as the minimum energy required to charge all BETs in the specified time remains the same. This increased p_{min} maximum at 10:00 is due to the additional BETs on the transit (or export) routes through (or out of) Austria, which are allowed to enter (or start in) Austria at around 5:00, after the night driving ban, and have to take a break in Austria at around 9:30 - 10:15 (Table 4.17 versus Table 4.18), which would otherwise have already taken place outside Austria (with a 70 km/h range of 315 km versus a 87 km/h range of 391.5 km in 4.5 h driving time in one go).
Above all, the number of necessary breaks of a single BET changes (less average speed corresponds to more necessary breaks due to constant maximum driving time in one go), whereby the p_{max} curve is increased over a large area (more BETs are plugged-in total in Austria (Table 4.15 and Table 4.17) versus Table 4.16 and Table 4.18), but usually (except the increased p_{min} maximum) nearly the same amount of energy is required in total (less per BET due to the shorter distance driven) to charge all BETs fully), which also increases (also due to the assumption that the installed capacities P_{limit} is the maximum of the p_{min} curve) the reserve power according to the simulation with decreasing average speed (if more or less consumption for the variation of the speeds is not taken into account).
This trend in reserve power can also be seen in Figure 4.19 for Austria as a whole and in Figure 4.21 for three selected NUTS3 regions. The values shown represent the reserve power in a 15 min time step, averaged over 2030 with public holidays. The slower the average speed of the BETs, the higher the simulated total reserve power for Austria.

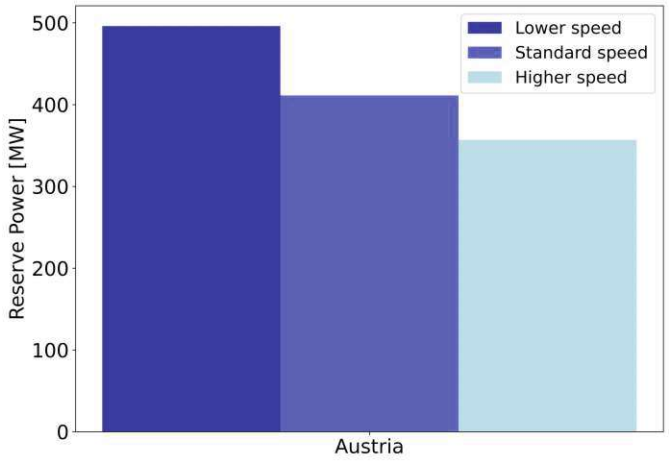

Figure 4.19: Reserve power in a 15 min time step averaged over the year 2030 with public holidays throughout Austria, depending on the average speed

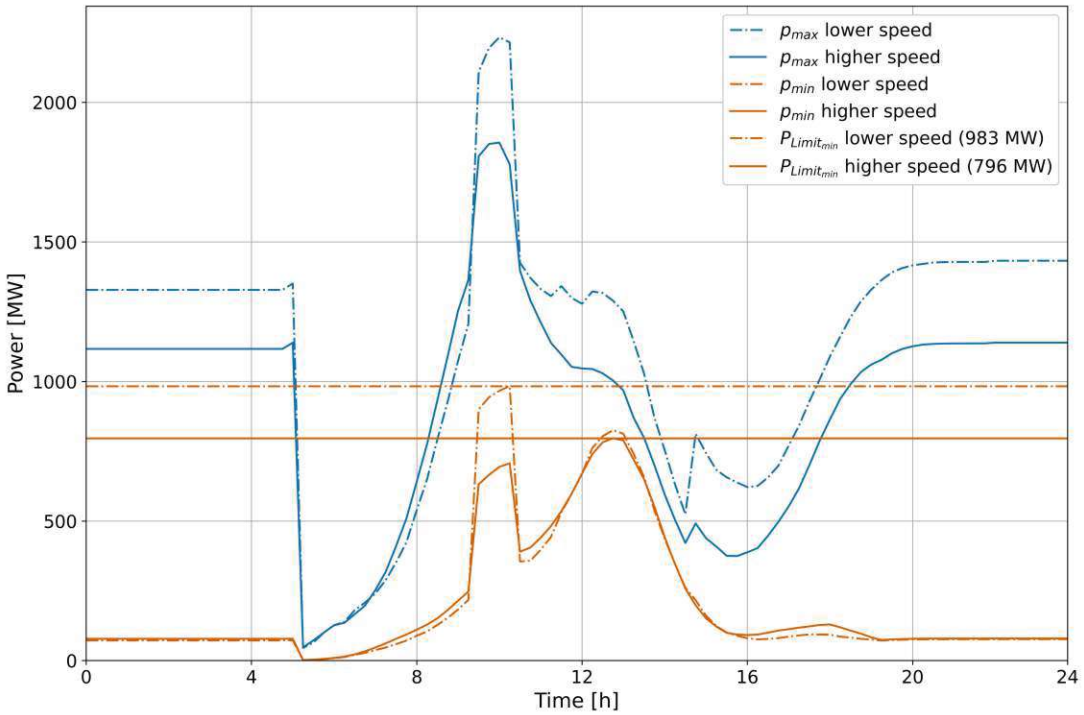

Figure 4.20: Comparison of different average speed combinations

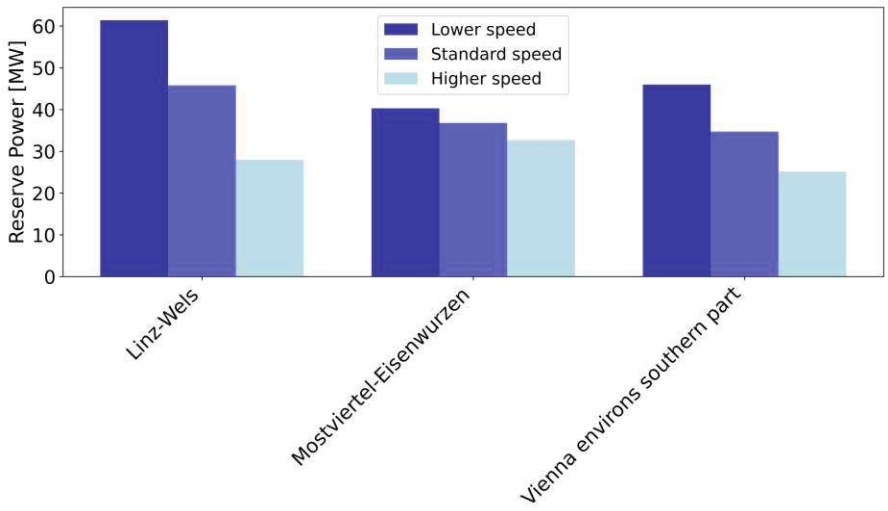

Figure 4.21: Reserve power in a 15 *min* time step averaged over the year 2030 with public holidays in three selected NUTS3 regions, depending on the average speed

The spatial distribution of the flexibility potential (or reserve power) is observed to change as a consequence of the varying average speeds, as illustrated in the subsequent figures (Figure 4.22 and Figure 4.23). The analysis is again carried out for an annual average Thursday in the respective 15 *min* time step. As anticipated, the reserve power Δp values (see Table 4.15 and Table 4.16) demonstrate a uniform increase for the first scenario with lower speeds of 70 km/h and 50 km/h and a decrease for the second scenario with higher speeds of 87 km/h and 67 km/h than assumed in the results section.
The most significant differences are in the regions crossed by the A1 freeway (Linz-Wels, Mostviertel-Eisenwurzen) and the southern environs of Vienna.

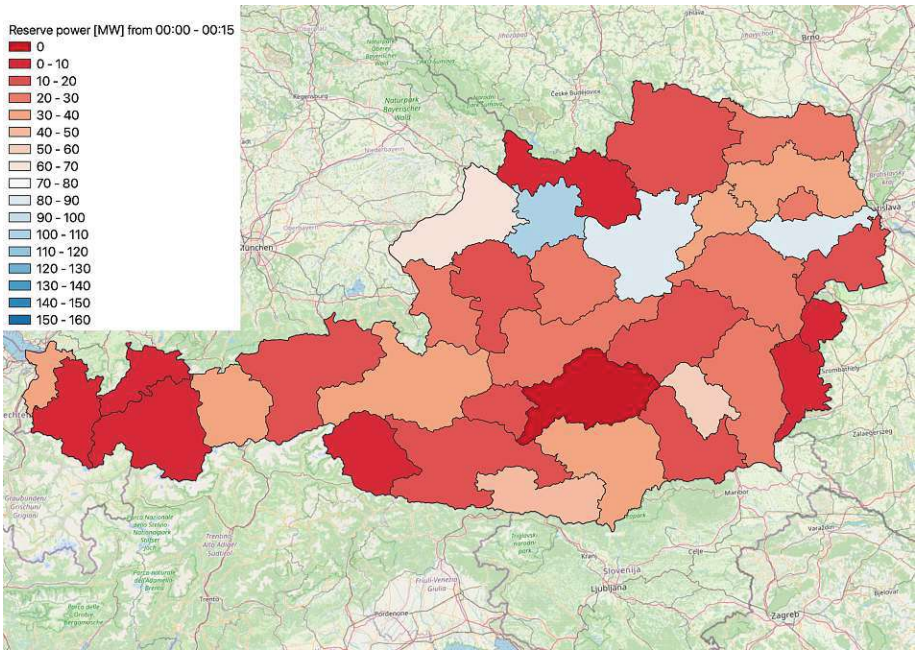

Figure 4.22: 70 km/h E-road, 50 km/h others average speed with limited installed charging capacity from 00:00 - 00:15

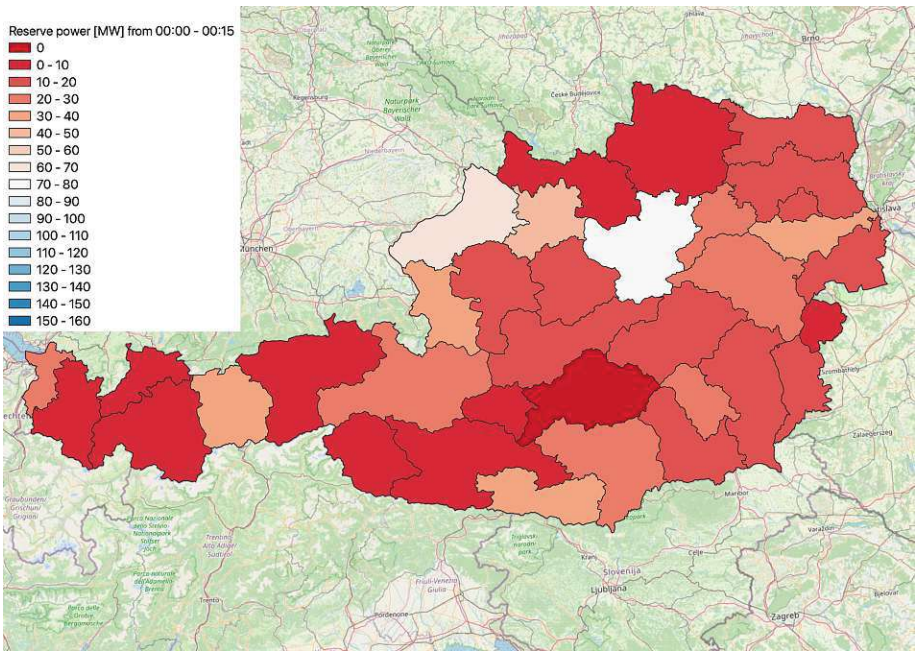

Figure 4.23: 87 km/h E-road, 67 km/h others average speed with limited installed charging capacity from 00:00 - 00:15

NUTS3 region	Δp $[MW]$	plugged-in BETs $[N]$
Linz-Wels	106.03	252.76
Mostviertel-Eisenwurzen	86.45	275.88
Vienna environs southern part	85.58	211.24
Außerfern	0.44	0.78
Central Burgenland	0.02	0.04
Western upper Styria	0.00	0.00
Austria in total	948.75	2387.32

Table 4.15: Highest and lowest reserve power Δp values from 00:00 - 00:15 with limited installed charging capacity with average speeds of 70 km/h on E-roads, 50 km/h on others

NUTS3 region	Δp $[MW]$	plugged-in BETs $[N]$
Mostviertel-Eisenwurzen	74.01	162.41
Innviertel	62.27	189.72
Linz-Wels	48.86	237.49
Außerfern	0.37	0.66
Central Burgenland	0.04	0.07
Western upper Styria	0.00	0.00
Austria in total	700.86	1898.64

Table 4.16: Highest and lowest reserve power Δp values from 00:00 - 00:15 with limited installed charging capacity with average speeds of 87 km/h on E-road, 67 km/h on others

NUTS3 region	Δp $[MW]$	plugged-in BETs $[N]$
Linz-Wels	23.99	356.88
Pinzgau-Pongau	22.11	83.72
Graz	16.14	145.44
Eastern Styria	0.00	121.86
Western and southern Styria	0.00	87.02
Innsbruck	0.00	105.84
Austria in total	142.57	3750.05

Table 4.17: Highest and lowest reserve power Δp values from 10:00 - 10:15 with limited installed charging capacity with average speeds of 70 km/h on E-roads, 50 km/h on others

NUTS3 region	Δp $[MW]$	plugged-in BETs $[N]$
Mostviertel-Eisenwurzen	24.65	134.28
Liezen	19.31	53.28
Salzburg and surroundings	17.34	146.20
Northern Burgenland	0.16	86.91
Western and southern Styria	0.13	108.23
Rhine Valley-Lake Constance region	0.00	84.37
Austria in total	188.24	3097.99

Table 4.18: Highest and lowest reserve power Δp values from 10:00 - 10:15 with limited installed charging capacity with average speeds of 87 km/h on E-road, 67 km/h on others

4.3.3 Limitation of installed capacities

Figure 4.24 shows the reserve power averaged over 2030 (including public holidays) for a 15 *min* time step, depending on the installed capacities.
Up to 1100 *MW* of installed capacity, the average reserve power rises steeply to 525 *MW* and up to 1300 *MW* installed capacity with a weaker gradient to 570 *MW* reserve power. Above 1300 *MW* of installed capacity, the reserve power increases only moderately, so an increase in installed capacity above 1300 *MW* is not in any meaningful proportion to the resulting increase in reserve power. This is because the available reserve power depends on the installed capacities and many factors, as described in the previous subsections. These are, for example, the number of BETs plugged in, the minimum charging power required to fully charge the individual BET within the specified charging time, the consumption and speed of the individual BET and the maximum technically possible charging power of the respective BET.

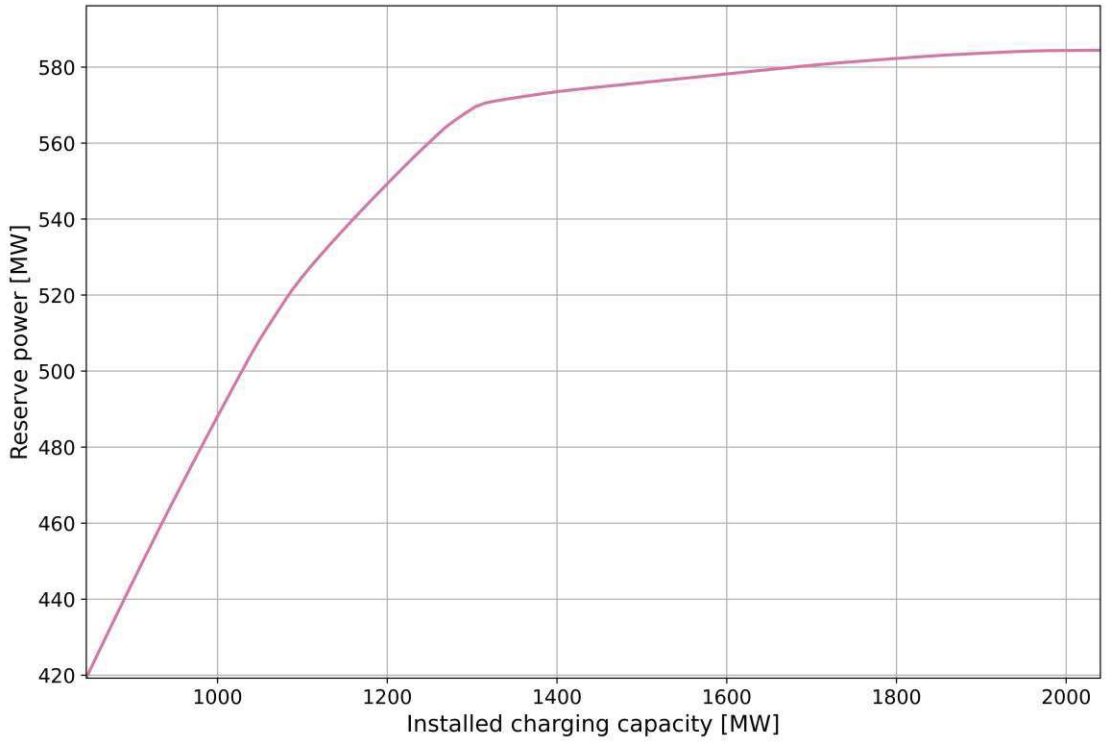

Figure 4.24: Reserve power Δp to installed capacity P_{Limit} throughout Austria averaged over the year 2030 based on a 15 *min* time step

5 Discussion

The discussion chapter of this thesis aims to synthesize the findings and answer the research question:

How is the flexibility of the charging power of BETs distributed throughout Austria regarding time and location?

By integrating the results from Chapter 4, this chapter not only confirms the temporal and spatial extent of the flexibility potential of reserve power from BETs but also provides additional insights from the analysis so that an answer to the question of whether this flexibility can be reliably utilized is found.

5.1 Temporal distribution of the flexibility

In winter, there is likely to be less reserve power (due to the higher average consumption of a BET (warming the battery, warming the cab, et cetera (Subsection 3.6.2))) than in summer, with logically constant limited installed capacities. More reserve power is generally available during the working week (Mon-Fri). From the beginning of the weekend, it decreases sharply and is very low on holidays/Sundays (due to the night driving ban combined with the weekend driving ban in Austria).
Within one day, there is a long stable plateau at night with 798.20 MW reserve power throughout Austria and a highly volatile phase during the day. In the volatile phase during the day, from 5:00 - 9:30 in the morning, the potential rises steadily from its daily low (Austria-wide on a weekday within a working week (Thursday) at 44.15 MW reserve power) to a high, but below the night-time level (609.13 MW) until from 9:30 - 10:15 the minimum charging power p_{min} required to charge all plugged-in BETs in the specified time reaches its maximum and the available reserve power shrinks to a local minimum (220.19 MW) due to the limitation of installed capacities throughout Austria and the abrupt drop in p_{max}, the maximum possible charging power, from 10:15 - 10:30. After another sharp increase after 10:30 to 583.02 MW reserve power across Austria, this drops again and reaches its Austria-wide minimum of 123.79 MW reserve power from 13:00 - 13:15. Until 14:45, the reserve power remains at a low level throughout Austria (< 191 MW) until it rises again from 14:45 (349.87 MW) and almost reaches the

stable night-time level again from 19:00 (774.90 *MW*).
This rhythm is repeated similarly on all days, albeit with different absolute values (especially between working days versus weekends/holidays). At night (especially on working days), this results in a readily usable, stable reserve power from electrified commercial traffic in Austria (assuming there are enough charging stations to keep the individual BET plugged in for its entire charging break); during the day, this is more difficult to assess.
Suppose enough capacity is installed to provide at least the minimum energy needed to fully charge each BET when it needs it in the specified time. In that case, the flexibility can be reliably used as reserve power during the day, except for the time ranges 9:30 - 10:30 and 12:00 - 14:45. If the installed capacities are expanded more than necessary, the time ranges 9:30 - 10:30 and 12:00 - 13:15 can also be utilized except in the Linz-Wels region. Even without expanding the installed capacities in the 9:30 - 10:30 period, this is likely to be suitable for flexibility use with at least 45 *MW* of reserve power.
However, the time range of at least 13:15 - 14:45 remains at a low reserve power level throughout Austria (189.94 – 247.47 *MW*), even if the installed capacities were to be expanded so that p_{max} would be reached at 13:15. In combination with an increase in the BET quota, however, the use of this time range would also be conceivable, as doubling the BET quota (and the correspondingly increased installed capacities) would also double the reserve power.

5.2 Spatial distribution of the flexibility

The analysis of the spatial distribution shows that the regions east of Tyrol will tend to have more reserve power from electrified commercial transport, and Tyrol and Vorarlberg will tend to have less (Figure 4.13). The following reserve power values are averaged over the entire year 2030 (including public holidays) based on a 15 *min* time step, calculated with a limitation of the installed capacities at $P_{Limit_{min}}$.
The Linz-Wels region (45.80 *MW*) is the most pronounced, ahead of the Mostviertel-Eisenwurzen (36.79 *MW*) and the environs south of Vienna (34.73 *MW*), all with limited installed capacities, as in the values mentioned here, as well as without limitation of the installed capacities, are most frequently among the top 3 with the most reserve power and also offer the highest available reserve power averaged over the entire year for a 15 *min* time step (Table 4.9). In addition to these regions, potential candidates for usable reserve power are Innviertel (27.41 *MW*), Klagenfurt-Villach (23.49 *MW*), Graz (18.24 *MW*), and St. Pölten (15.84 *MW*). According to the simulation, Vorarlberg and Tyrol (except Innsbruck) will not offer reliably utilizable flexibility through electrified commercial transport in 2030 (Vorarlberg: AT341: 2.73 *MW*, AT342: 8.94 *MW*; Tyrol without Innsbruck: AT333: 0.61 *MW*, AT334: 2.63 *MW*, AT335: 4.82 *MW*).

As expected, the regions with a lot of interregional freeway HDVs traffic are potentially much more interesting for reliable use of the flexibility potential, whereby the pure number of plugged-in BETs is not directly proportional to the expected reserve power.

5.3 Utilization of the flexibility potential

The maximum technically feasible charging speed of an individual BET, the BET quota across Europe, and the installed capacities in Austria are the key factors determining how much reserve power will actually be available by 2030. Therefore, predictions regarding absolute values should be approached with caution. Can this flexibility be reliably utilized? There are varying answers to this question. Overall, in Austria, the answer is no; it cannot be relied upon at all times.
However, it can be used reliably during predictable time frames on weekdays, specifically from 7:00 - 9:30, 10:30 - 12:00, and 14:45 - 4:45, in certain regions such as Linz-Wels, Mostviertel-Eisenwurzen, and the southern areas of Vienna.

6 Conclusions

This chapter draws conclusions based on the discussion and its relevance to the research question. It looks at what the model is suitable for, what limitations it is subject to, and where there is potential for improvement. Finally, suggestions are made for further enhancements of the work and the model it contains.

6.1 Modeling and simulation of the flexibility potential of BETs in Austria in 2030

This thesis aims to develop a model that simulates the electrified truck traffic in Austria and calculates an assumption about the flexibility potential in 2030. From the results of this thesis, it can be summarized that a large number of connected BETs in a region does not necessarily mean a lot of flexibility potential. In addition to other factors mentioned above, this primarily depends on the installed capacities, how fully utilized these are, and how long the respective BET can remain plugged in. However, regions with few plugged-in BETs tend to be associated with little flexibility potential, as the basis for a high flexibility potential is missing here.
Existing flexibility potential is primarily associated with the strength of the industrial production location of the respective region [62], as well as the infrastructure of the roads [63], the transit or freeway routes. At least a correlation exists with the truck traffic density on these freeways [64]. In addition, limiting the installed capacities with a limit at the p_{min} weekly maximum means that regions with high volatility of the p_{min} curve or peaks and high p_{min} maxima have relatively more reserve capacity available at times than regions with a very flat p_{min} curve.
In this work, the bottom-up model structure has proven itself so that each BET is simulated individually on one of the synthetic routes affecting Austria, with its own Gaussian-distributed start time and the energy requirements resulting from the pauses added up per time step. The following things can be read from this simulation. In addition to the relative number of plugged-in BETs per region and time step (can also be extended from the existing 15 min to 1 s resolution), the relative spatial and temporal distribution of the flexibility potential can also be read out and displayed. The examined sensitivities of the flexibility potential can be understood.

For example, changes in average speed shift the charging breaks in terms of time and spatial location, resulting in a shift in the flexibility potential. About the individual BET, this means that at slower speeds (as long as a reduction in consumption due to the change in speed is not noticeable), it has to take more breaks per route, with similar energy requirements for the entire route, due to the legal limit on driving time and not necessarily due to the range of the BET. This can significantly impact the actual flexibility potential in Austria, especially for BETs that travel on the many transit routes through Austria.
In addition, seasonal differences, which exist solely due to differences in consumption (truck traffic density hardly differs seasonally), can be seen. In addition, the relationship between installed capacity and expected flexibility can be presented and interpreted (also possible at NUTS3 level or node level with certain uncertainties due to the inaccuracies in the data basis of the synthesized routes Subsection 3.1.2).
The following problems and inconsistencies exist with the model. Adding up the flexibility in 15 *min* time steps of a time hour results in certain inaccuracies. For example, if a BET is plugged in from 10:07 - 10:52, it also counts in the time step from 10:00 - 10:15, as well as 10:45 - 11:00 as a plugged-in BET. This causes an inaccuracy which, however, decreases with longer pauses. Since every second break of a BET on a route must be at least 9 *h* long and a night break must also be at least 7 *h* long due to the night driving ban in Austria, this inaccuracy is smaller overall than shown in this example and is calculable.
In addition, the start times are considered to be normally distributed over the number of individual starts. In reality, however, the start times may depend much more on the actual type of transportation. For example, urban deliveries to markets will occur before the market opens. However, deliveries to the production company will take place during regular business hours. This was not taken into account in the modeling.
In the connection between an ASFINAG counting station [29], which provides the relative number of trucks per route based on one day of the year, and a node of the respective route synthesized by Speth et al. [28], there are sometimes large distances, since counting station and node are not always located next to each other or for some nodes there is no directly corresponding counting station (see Figure 3.4). This results in the fact that the temporal classification of the trucks within a week (i.e., the calculation of the trucks/24h on a route depending on the day of the week) is subject to a particular uncertainty or error.
In addition, the absolute figures of the flexibility potential are subject to errors simply because the modeling does not take charging strategies into account, and the "human factor" is not taken into account either, for example, through individual charging decisions, individual consumption, actual speeds driven, et cetera.
What could be improved is that so far, it is assumed that each BET can load at the node where the break takes place due to the limited travel time. This error can be considered negligible since the local resolution here is at NUTS3 level. However, there is also a

specific timing error. This point can be improved by adding a map of possible charging locations to the model. The modeling is also based on fleets and routes. This means exemptions relating to individual truck drivers' driving times cannot be considered. Also, despite the ban on night driving, no exemptions for driving at night were taken into account. This can cause an error in the driving time within a day. The allocation of the individual days is based on the traffic count and is therefore less affected by this.
In the summaries for 2030, the insertion of public holidays is imprecise and causes specific errors. According to the traffic count [29], a public holiday corresponds to a Sunday. The year was built from a simulated annual average week, which means that on public holidays that are within a working week, there is a jump in the traffic count and in the p_{min} as well as p_{max} curve between the previous day 23:59 and the inserted public holiday 00:00 and also between the public holiday 23:59 and the following weekday 00:00. These jumps do not exist in reality, but the day before and the day after will rather have lower p_{min} and p_{max} curves than assumed. This will result in a slightly lower annual value than calculated when considered in the model.
The model and its results have limitations. One is that the p_{min} calculation is based on the charging time of a BET. The calculation of p_{max} is based on the number of plugged-in BETs at the respective time. If flexibility is now utilized by increasing the charging power, the BET is charged faster than the minimum time required, which means that less charging power than p_{min} is required in the next time step in order to continue charging the BET during the entire pause time, as it would otherwise be fully charged earlier than the pause is long. On the other hand, the maximum usable charging power p_{max} will no longer be available earlier. This means that if a lot of reserve power is used from 00:00 - 00:15, there will be no more flexibility or reserve power available from 00:15 for the corresponding BETs that are fully charged earlier (if not also limited by the limited installed capacities). In principle, this means that the BET can only be charged up to 100 %. If this BET is fully charged by using the flexibility and full charging power, it is no longer available for using the flexibility and therefore changes both the p_{min} and p_{max} curve downwards. Therefore, the available reserve power must be considered dynamically when used.
It should also be borne in mind that if BETs are only allowed to be plugged in for the charging time actually required due to the limited availability of charging stations, the resulting reserve power Δp changes fundamentally, as the long charging times, in particular, would be significantly reduced (at night, et cetera) or, in case of doubt, there may no longer be any flexibility at all.
It is assumed that each BET starts with $SoC = 100$ % and is recharged to $SoC = 100$ % at each break to simplify matters. This must be borne in mind when considering the results, as in reality, the battery is also started with less SoC and is not necessarily fully recharged at every break if the charging process is terminated early. This influences the level of the p_{min} if a full charge is nevertheless desired (this must be higher due to the shorter time), as well as on the p_{max}, as the corresponding BET is no longer

plugged in earlier and is therefore no longer available for the maximum charging power. For further simplification, a ban on night-time truck driving is also assumed for all locations (including outside Austria).
Suppose the model is to be used for calculations outside Austria. In that case, it must be examined more closely and adapted if necessary, as a night-time driving ban for trucks exists in Europe in Austria, Switzerland, Liechtenstein, and England, for example, but not uniformly. It is also assumed that the legally prescribed driving times are adhered to everywhere. As this may not be the case in reality, this can lead to flexibility shifts in time and location. The modeling used as a fleet calculation, with fleet sizes often < 0.5 BETs per fleet on a route one day, can lead to inaccuracies. It is assumed that this essentially balances out in the total of all routes and fleets but still leads to statistical uncertainty.

6.2 Further Work

This section provides ideas for further work to overcome methodological limitations. It is beneficial to incorporate various charging strategies and optimize charging infrastructure in the modeling process to enhance the accuracy of predictions. Additionally, integrating actual charging locations into the model can significantly improve location and time accuracy. A more precise assessment of driving speeds is also crucial, as these speeds greatly affect reserve power values. For example, factors such as transit traffic in Austria can lead to additional breaks or fewer stops, depending on the speed. Furthermore, it is essential to account for differences in energy consumption at varying speeds to refine the analysis.
Furthermore, the start times should undergo a sensitivity analysis and be adjusted as needed. For a comprehensive analysis across Europe using this model, it is essential to incorporate the legal requirements of each country, such as night driving bans and driving time regulations. Additionally, any inaccuracies arising from the summation during the time steps, as detailed in Section 6.1, should be calculated and corrected.
It is advisable to conduct a detailed examination of the individual NUTS3 regions that may be considered to enhance the analysis of the flexibility potential of electrified trucks in Austria. Each region has specific differences, particularly in timing, which can affect usability. Additionally, establishing a connection between existing and required flexibilities is important.
In summary, this modeling provides valuable insights to assess the expected flexibility potential in Austria for 2030 and beyond, serving as a foundation for further investigation and utilization.

Appendix

Appendix A. Supplementary material

NUTS region number	NUTS region name
AT1	East Austria
AT11	Burgenland
AT111	Central Burgenland
AT112	Northern Burgenland
AT113	Southern Burgenland
AT12	Lower Austria
AT121	Mostviertel-Eisenwurzen
AT122	Lower Austria-South
AT123	St. Pölten
AT124	Waldviertel
AT125	Weinviertel
AT126	Vienna environs northern part
AT127	Vienna environs southern part
AT13	Vienna
AT130	Vienna
AT2	South Austria
AT21	Carinthia
AT211	Klagenfurt-Villach
AT212	Upper Carinthia
AT213	Lower Carinthia
AT22	Styria
AT221	Graz
AT222	Liezen
AT223	Eastern upper Styria
AT224	East Styria
AT225	West and South Styria
AT226	Western upper Styria

Table A1: Eastern and southern NUTS regions in Austria [65]

NUTS region number	NUTS region name
AT3	West Austria
AT31	Upper Austria
AT311	Innviertel
AT312	Linz-Wels
AT313	Mühlviertel
AT314	Steyr-Kirchdorf
AT315	Traunviertel
AT32	Salzburg
AT321	Lungau
AT322	Pinzgau-Pongau
AT323	Salzburg and surroundings
AT33	Tyrol
AT331	Außerfern
AT332	Innsbruck
AT333	East Tyrol
AT334	Tyrolean Oberland
AT335	Tyrolean Unterland
AT34	Vorarlberg
AT341	Bludenz-Bregenzer Wald
AT342	Rhine Valley-Lake Constance region

Table A2: Western NUTS regions in Austria [65]

Appendix B. Directory of resources

Resources	Used for	Where
ChatGPT	Creating code samples for plots, help with code issues	Total work
Deepl	Help with translation and spell checking	Total work
Grammarly	Spell checking and correcting the grammatics	Total work

Table A3: Directory of resources

Bibliography

[1] M.-T. Huang and P.-M. Zhai, "Achieving Paris Agreement temperature goals requires carbon neutrality by middle century with far-reaching transitions in the whole society," en, *Advances in Climate Change Research*, vol. 12, no. 2, pp. 281–286, Apr. 2021, ISSN: 16749278. DOI: 10.1016/j.accre.2021.03.004. [Online]. Available: https://linkinghub.elsevier.com/retrieve/pii/S1674927821000435 (visited on 12/30/2024) (cit. on p. 1).

[2] E. Ciotti, M. Tritoni, D. Pelosi, and L. Barelli, "Management Optimization of Fuel Cell Electric Bus Fleet in Urban Areas," en, in *2023 AEIT International Annual Conference (AEIT)*, Rome, Italy: IEEE, Oct. 2023, pp. 1–6, ISBN: 978-88-87237-60-3. DOI: 10.23919/AEIT60520.2023.10330322. [Online]. Available: https://ieeexplore.ieee.org/document/10330322/ (visited on 12/30/2024) (cit. on p. 1).

[3] W. Siebenpfeiffer, Ed., *Heavy-Duty-, On- und Off-Highway-Motoren 2019: Zukünftige Herausforderungen 14. Internationale MTZ-Fachtagung Großmotoren* (Proceedings), en. Wiesbaden: Springer Fachmedien Wiesbaden, 2020, ISBN: 978-3-658-31370-8 978-3-658-31371-5. DOI: 10.1007/978-3-658-31371-5. [Online]. Available: http://link.springer.com/10.1007/978-3-658-31371-5 (visited on 12/30/2024) (cit. on p. 1).

[4] F. López-Ramos, S. Nasini, and M. H. Sayed, "An integrated planning model in centralized power systems," en, *European Journal of Operational Research*, vol. 287, no. 1, pp. 361–377, Nov. 2020, ISSN: 03772217. DOI: 10.1016/j.ejor.2020.05.006. [Online]. Available: https://linkinghub.elsevier.com/retrieve/pii/S0377221720304173 (visited on 12/30/2024) (cit. on p. 1).

[5] M. Huber, D. Dimkova, and T. Hamacher, "Integration of wind and solar power in Europe: Assessment of flexibility requirements," en, *Energy*, vol. 69, pp. 236–246, May 2014, ISSN: 03605442. DOI: 10.1016/j.energy.2014.02.109. [Online]. Available: https://linkinghub.elsevier.com/retrieve/pii/S0360544214002680 (visited on 12/27/2024) (cit. on pp. 2, 6).

[6] D. Papadaskalopoulos *et al.*, "Quantifying the Potential Economic Benefits of Flexible Industrial Demand in the European Power System," en, *IEEE Transactions on Industrial Informatics*, vol. 14, no. 11, pp. 5123–5132, Nov. 2018, ISSN: 1551-3203, 1941-0050. DOI: 10.1109/TII.2018.2811734. [Online]. Available: https://ieeexplore.ieee.org/document/8309292/ (visited on 12/27/2024) (cit. on pp. 2, 5, 6).

[7] M. Poncela, A. Purvins, and S. Chondrogiannis, "Pan-European Analysis on Power System Flexibility," en, *Energies*, vol. 11, no. 7, p. 1765, Jul. 2018, ISSN: 1996-1073. DOI: 10.3390/en11071765. [Online]. Available: https://www.mdpi.com/1996-1073/11/7/1765 (visited on 12/27/2024) (cit. on pp. 2, 6).

[8] H. Ü. Yilmaz, D. Keles, A. Chiodi, R. Hartel, and M. Mikulić, "Analysis of the power-to-heat potential in the European energy system," en, *Energy Strategy Reviews*, vol. 20, pp. 6–19, Apr. 2018, ISSN: 2211467X. DOI: 10.1016/j.esr.2017.12.009. [Online]. Available: https://linkinghub.elsevier.com/retrieve/pii/S2211467X17300871 (visited on 12/27/2024) (cit. on pp. 2, 6).

[9] A. Forouli *et al.*, "Assessment of Demand Side Flexibility in European Electricity Markets: A Country Level Review," en, *Energies*, vol. 14, no. 8, p. 2324, Apr. 2021, ISSN: 1996-1073. DOI: 10.3390/en14082324. [Online]. Available: https://www.mdpi.com/1996-1073/14/8/2324 (visited on 12/27/2024) (cit. on pp. 2, 6).

[10] J. D. Peper, J. Schmeing, and U. Häger, "Spatio-temporal electric vehicle charging optimization considering distribution grid constraints and flexible electricity prices," en, in *2023 19th International Conference on the European Energy Market (EEM)*, Lappeenranta, Finland: IEEE, Jun. 2023, pp. 1–6, ISBN: 9798350312584. DOI: 10.1109/EEM58374.2023.10161970. [Online]. Available: https://ieeexplore.ieee.org/document/10161970/ (visited on 12/30/2024) (cit. on p. 2).

[11] H. Wu, T. Huang, S. Conti, and E. Bompard, "A Framework for Assessing Electricity Market Performance under Different Bidding Zone Configurations," en, *Energies*, vol. 17, no. 11, p. 2743, Jun. 2024, ISSN: 1996-1073. DOI: 10.3390/en17112743. [Online]. Available: https://www.mdpi.com/1996-1073/17/11/2743 (visited on 12/30/2024) (cit. on p. 2).

[12] C. Gaete-Morales, J. Jöhrens, F. Heining, and W.-P. Schill, "Power sector effects of alternative options for de-fossilizing heavy-duty vehicles—Go electric, and charge smartly," en, *Cell Reports Sustainability*, vol. 1, no. 6, p. 100 123, Jun. 2024, ISSN: 29497906. DOI: 10.1016/j.crsus.2024.100123. [Online]. Available: https://linkinghub.elsevier.com/retrieve/pii/S2949790624001964 (visited on 12/30/2024) (cit. on p. 2).

[13] K. Ginigeme and Z. Wang, "Distributed Optimal Vehicle-To-Grid Approaches With Consideration of Battery Degradation Cost Under Real-Time Pricing," en, *IEEE Access*, vol. 8, pp. 5225–5235, 2020, ISSN: 2169-3536. DOI: 10.1109/ACCESS.2019.2963692. [Online]. Available: https://ieeexplore.ieee.org/document/8949354/ (visited on 12/30/2024) (cit. on p. 2).

[14] V. Gass, J. Schmidt, F. Strauss, and E. Schmid, "Assessing the economic wind power potential in Austria," en, *Energy Policy*, vol. 53, pp. 323–330, Feb. 2013, ISSN: 03014215. DOI: 10.1016/j.enpol.2012.10.079. [Online]. Available: https://linkinghub.elsevier.com/retrieve/pii/S0301421512009640 (visited on 12/30/2024) (cit. on p. 2).

[15] C. Mikovits *et al.*, "A Spatially Highly Resolved Ground Mounted and Rooftop Potential Analysis for Photovoltaics in Austria," en, *ISPRS International Journal of Geo-Information*, vol. 10, no. 6, p. 418, Jun. 2021, ISSN: 2220-9964. DOI: 10.3390/ijgi10060418. [Online]. Available: https://www.mdpi.com/2220-9964/10/6/418 (visited on 12/30/2024) (cit. on p. 2).

[16] F. Ziel, R. Steinert, and S. Husmann, "Forecasting day ahead electricity spot prices: The impact of the EXAA to other European electricity markets," en, *Energy Economics*, vol. 51, pp. 430–444, Sep. 2015, arXiv:1501.00818 [q-fin], ISSN: 01409883. DOI: 10.1016/j.eneco.2015.08.005. [Online]. Available: http://arxiv.org/abs/1501.00818 (visited on 12/30/2024) (cit. on p. 2).

[17] M. Raskopina, "Flexibility Products and their Future Opportunities for the Austrian Electricity Market," en, (cit. on p. 2).

[18] C. Zöphel, S. Schreiber, T. Müller, and D. Möst, "Which Flexibility Options Facilitate the Integration of Intermittent Renewable Energy Sources in Electricity Systems?" en, *Current Sustainable/Renewable Energy Reports*, vol. 5, no. 1, pp. 37–44, Mar. 2018, ISSN: 2196-3010. DOI: 10.1007/s40518-018-0092-x. [Online]. Available: http://link.springer.com/10.1007/s40518-018-0092-x (visited on 12/27/2024) (cit. on pp. 4, 7).

[19] L. De Vries and R. Verzijlbergh, "How Renewable Energy is Reshaping Europes Electricity Market Design," en, *Economics of Energy & Environmental Policy*, vol. 7, no. 2, Apr. 2018, ISSN: 21605882. DOI: 10.5547/2160-5890.7.2.ldev. [Online]. Available: http://www.iaee.org/en/publications/eeeparticle.aspx?id=227 (visited on 12/27/2024) (cit. on p. 5).

[20] C. K. Chyong, M. Pollitt, D. Reiner, and C. Li, "Modelling flexibility requirements in deep decarbonisation scenarios: The role of conventional flexibility and sector coupling options in the European 2050 energy system," en, *Energy Strategy Reviews*, vol. 52, p. 101 322, Mar. 2024, ISSN: 2211467X. DOI: 10.1016/j.esr.2024.101322. [Online]. Available: https://linkinghub.elsevier.com/retrieve/pii/S2211467X24000294 (visited on 12/27/2024) (cit. on pp. 5, 6).

[21] V. Vita, C. Christodoulou, I. Zafeiropoulos, I. Gonos, M. Asprou, and E. Kyriakides, "Evaluating the Flexibility Benefits of Smart Grid Innovations in Transmission Networks," en, *Applied Sciences*, vol. 11, no. 22, p. 10 692, Nov. 2021, ISSN: 2076-3417. DOI: 10.3390/app112210692. [Online]. Available: https://www.mdpi.com/2076-3417/11/22/10692 (visited on 12/27/2024) (cit. on p. 6).

[22] R. Lu, S. H. Hong, and X. Zhang, "A Dynamic pricing demand response algorithm for smart grid: Reinforcement learning approach," en, *Applied Energy*, vol. 220, pp. 220–230, Jun. 2018, ISSN: 03062619. DOI: 10.1016/j.apenergy.2018.03.072. [Online]. Available: https://linkinghub.elsevier.com/retrieve/pii/S0306261918304112 (visited on 12/27/2024) (cit. on p. 6).

[23] A. Pepiciello and A. Vaccaro, "The Role of Vehicle to Grid Technology for Enhancing Power Distribution System Flexibility," en, in *2022 IEEE International Workshop on Metrology for Automotive (MetroAutomotive)*, Modena, Italy: IEEE, Jul. 2022, pp. 24–29, ISBN: 978-1-66546-689-9. DOI: 10.1109/MetroAutomotive54295.2022.9855066. [Online]. Available: https://ieeexplore.ieee.org/document/9855066/ (visited on 12/27/2024) (cit. on p. 7).

[24] N. Refa, Geelen, Daphne, and Spiering, Ralf, "SMART CHARGING ELECTRIC VEHICLES BASED ON A FLEXIBILITY MARKET," en, *International Conference on Electricity Distribution*, no. 1533, 2019 (cit. on p. 7).

[25] V. Barthel, J. Schlund, P. Landes, V. Brandmeier, and M. Pruckner, "Analyzing the Charging Flexibility Potential of Different Electric Vehicle Fleets Using Real-World Charging Data," en, *Energies*, vol. 14, no. 16, p. 4961, Aug. 2021, ISSN: 1996-1073. DOI: 10.3390/en14164961. [Online]. Available: https://www.mdpi.com/1996-1073/14/16/4961 (visited on 12/28/2024) (cit. on p. 7).

[26] C. Will and F. Ocker, "Flexibility Potential of Smart Charging Electric Trucks and Buses," en, *World Electric Vehicle Journal*, vol. 15, no. 2, p. 56, Feb. 2024, ISSN: 2032-6653. DOI: 10.3390/wevj15020056. [Online]. Available: https://www.mdpi.com/2032-6653/15/2/56 (visited on 12/28/2024) (cit. on p. 8).

[27] C. Loschan, D. Schwabeneder, G. Lettner, and H. Auer, "Flexibility potential of aggregated electric vehicle fleets to reduce transmission congestions and redispatch needs: A case study in Austria," en, *International Journal of Electrical Power & Energy Systems*, vol. 146, p. 108 802, Mar. 2023, ISSN: 01420615. DOI: 10.1016/j.ijepes.2022.108802. [Online]. Available: https://linkinghub.elsevier.com/retrieve/pii/S0142061522007980 (visited on 12/28/2024) (cit. on p. 8).

[28] D. Speth, V. Sauter, P. Plötz, and T. Signer, "Synthetic European road freight transport flow data based on ETISplus," en, vol. 1, Sep. 2021, Publisher: Mendeley Data. DOI: 10.17632/py2zkrb65h.1. [Online]. Available: https://data.

mendeley.com/datasets/py2zkrb65h/1 (visited on 10/15/2024) (cit. on pp. 10, 12, 19, 30, 31, 65).

[29] *Verkehrsentwicklung*, de. [Online]. Available: https://www.asfinag.at/verkehr-sicherheit/verkehrszaehlung/ (visited on 10/16/2024) (cit. on pp. 10, 19, 30, 65, 66).

[30] *Übersicht - Eurostat*. [Online]. Available: https://ec.europa.eu/eurostat/de/web/nuts (visited on 10/17/2024) (cit. on p. 11).

[31] *Grundsätze - Eurostat*. [Online]. Available: https://ec.europa.eu/eurostat/de/web/nuts/principles (visited on 10/17/2024) (cit. on p. 11).

[32] N. G. Van Kampen, "Stochastic Processes in Physics and Chemistry," eng, in *Stochastic Processes in Physics and Chemistry*, The Netherlands: Elsevier Science & Technology, 2007, ISBN: 978-0-444-52965-7 (cit. on p. 16).

[33] *Lkw-Fahrverbote in österreich: Überblick*, de-AT. [Online]. Available: https://www.wko.at/transport/lkw-fahrverbote-oesterreich-ueberblick (visited on 10/16/2024) (cit. on pp. 16, 28).

[34] *PyCharm: Die Python-IDE für Data Science und Webentwicklung*, de. [Online]. Available: https://www.jetbrains.com/de-de/pycharm/ (visited on 12/17/2024) (cit. on p. 26).

[35] *Python.org*, en, Dec. 2024. [Online]. Available: https://www.python.org/ (visited on 12/17/2024) (cit. on p. 26).

[36] *Ast — Abstract Syntax Trees*, en. [Online]. Available: https://docs.python.org/3/library/ast.html (visited on 12/17/2024) (cit. on p. 27).

[37] *Pandas: Powerful data structures for data analysis, time series, and statistics*. [Online]. Available: https://pandas.pydata.org (visited on 12/17/2024) (cit. on p. 27).

[38] *Numpy: Fundamental package for array computing in Python* (cit. on p. 27).

[39] *Random — Generate pseudo-random numbers*, en. [Online]. Available: https://docs.python.org/3/library/random.html (visited on 12/17/2024) (cit. on p. 27).

[40] *Datetime — Basic date and time types*, en. [Online]. Available: https://docs.python.org/3/library/datetime.html (visited on 12/17/2024) (cit. on p. 27).

[41] *Multiprocessing: Backport of the multiprocessing package to Python 2.4 and 2.5*. [Online]. Available: http://code.google.com/p/python-multiprocessing (visited on 12/17/2024) (cit. on p. 27).

[42] *TIME-python: Implementation of TIME*. [Online]. Available: https://github.com/DelinteNicolas/TIME (visited on 12/17/2024) (cit. on p. 27).

[43] *Os — Miscellaneous operating system interfaces*, en. [Online]. Available: https://docs.python.org/3/library/os.html (visited on 12/17/2024) (cit. on p. 27).

[44] *Matplotlib: Python plotting package*. [Online]. Available: https://matplotlib.org (visited on 12/17/2024) (cit. on p. 27).

[45] *Json — JSON encoder and decoder*, en. [Online]. Available: https://docs.python.org/3/library/json.html (visited on 12/17/2024) (cit. on p. 27).

[46] *Pickle — Python object serialization*, en. [Online]. Available: https://docs.python.org/3/library/pickle.html (visited on 12/17/2024) (cit. on p. 27).

[47] *Spatial without Compromise · QGIS Web Site*, en. [Online]. Available: https://www.qgis.org/ (visited on 12/17/2024) (cit. on p. 27).

[48] *Territorial units for statistics (NUTS) - GISCO - Eurostat*. [Online]. Available: https://ec.europa.eu/eurostat/web/gisco/geodata/statistical-units/territorial-units-statistics (visited on 12/17/2024) (cit. on p. 27).

[49] OpenStreetMap contributors, *Planet dump retrieved from https://planet.osm.org*, 2024. [Online]. Available: https://www.openstreetmap.org (visited on 10/01/2024) (cit. on p. 27).

[50] *Arbeitszeittabelle: Lenkzeiten*, de-AT. [Online]. Available: https://www.wko.at/oe/transport-verkehr/gueterbefoerderungsgewerbe/arbeitszeittabelle-lenkzeiten (visited on 12/18/2024) (cit. on p. 28).

[51] W. et al., *Lkw-Geschwindigkeiten auf Autobahnen*, German. [Online]. Available: https://wien.arbeiterkammer.at/interessenvertretung/umweltundverkehr/verkehr/strasse/Auswirkungen_aufs_Klima.pdf (visited on 11/02/2024) (cit. on p. 28).

[52] A. Pumberger, T. Fessl, and N. Authried, *Lkw-Geschwindigkeitsverhalten auf Autobahnen: Erhebung und Analyse der Lkw-Geschwindigkeiten auf ausgewählten Streckenabschnitten österreichischer Autobahnen ; erstellt vom Kuratorium für Verkehrssicherheit* (Verkehr und Infrastruktur 44), de. Wien: Kammer für Arbeiter und Angestellte für Wien, 2011, ISBN: 978-3-7063-0405-4 (cit. on pp. 28, 29).

[53] D. Speth, P. Plötz, S. Funke, and E. Vallarella, "Public fast charging infrastructure for battery electric trucks—a model-based network for Germany," en, *Environmental Research: Infrastructure and Sustainability*, vol. 2, no. 2, p. 025 004, Jun. 2022, Publisher: IOP Publishing, ISSN: 2634-4505. DOI: 10.1088/2634-4505/ac6442. [Online]. Available: https://dx.doi.org/10.1088/2634-4505/ac6442 (visited on 11/04/2024) (cit. on p. 29).

[54] A. K. Breed, D. Speth, and P. Plötz, "CO2 fleet regulation and the future market diffusion of zero-emission trucks in Europe," *Energy Policy*, vol. 159, p. 112 640, Dec. 2021, ISSN: 0301-4215. DOI: 10.1016/j.enpol.2021.112640. [Online]. Available: https://www.sciencedirect.com/science/article/pii/S030142152100505X (visited on 11/04/2024) (cit. on p. 29).

[55] W. Shoman, S. Yeh, F. Sprei, P. Plötz, and D. Speth, "Battery electric long-haul trucks in Europe: Public charging, energy, and power requirements," *Transportation Research Part D: Transport and Environment*, vol. 121, p. 103 825, Aug. 2023, ISSN: 1361-9209. DOI: 10.1016/j.trd.2023.103825. [Online]. Available: https://www.sciencedirect.com/science/article/pii/S1361920923002225 (visited on 11/04/2024) (cit. on p. 29).

[56] Chrstian Will and Dr. Fabian Ocker, *Flexibility marketing options for charging processes of electric medium-duty and heavy-duty commercial vehicles*, en, Jun. 2022. [Online]. Available: https://tennet-drupal.s3.eu-central-1.amazonaws.com/default/2022-11/Daimler%20Truck%20TenneT%20Feasibility%20Study.pdf (visited on 11/04/2024) (cit. on p. 30).

[57] *Die Zukunft liegt im Megawatt-Laden*, de. [Online]. Available: https://de.heliox-energy.com/blog/megawattladen (visited on 11/04/2024) (cit. on p. 30).

[58] G. Dou *et al.*, "Analysis of the Actual Usage and Emission Reduction Potential of Electric Heavy-Duty Trucks: A Case Study of a Steel Plant," *Atmosphere*, vol. 14, p. 1562, Oct. 2023. DOI: 10.3390/atmos14101562 (cit. on p. 30).

[59] *Volvo's heavy-duty electric truck is put to the test: Excels in both range and energy efficiency*, en. [Online]. Available: https://www.volvotrucks.com/en-en/news-stories/press-releases/2022/jan/volvos-heavy-duty-electric-truck-is-put-to-the-test-excels-in-both-range-and-energy-efficiency.html (visited on 11/04/2024) (cit. on p. 30).

[60] *MAN Elektro-Lkw: Modelle in der übersicht — MAN AT*, de. [Online]. Available: https://www.man.eu/at/de/lkw/elektro-lkw/uebersicht.html (visited on 11/04/2024) (cit. on p. 30).

[61] D. Speth, V. Sauter, P. Plötz, and T. Signer, "Synthetic European road freight transport flow data," en, *Data in Brief*, vol. 40, p. 107 786, Feb. 2022, ISSN: 23523409. DOI: 10.1016/j.dib.2021.107786. [Online]. Available: https://linkinghub.elsevier.com/retrieve/pii/S235234092101060X (visited on 11/10/2023) (cit. on p. 31).

[62] *INDUSTRIEMAGAZIN — Ranking: Wirtschaftsstärkste Bundesländer österreichs 2023*, de. [Online]. Available: https://industriemagazin.at/artikel/wie-gut-ist-ihr-bundesland/ (visited on 12/25/2024) (cit. on p. 64).

[63] *Straßensystem österreich — i-vignette.com — i-Vignette*. [Online]. Available: https://i-vignette.com/de-de/laender/oesterreich/strassensystem (visited on 12/25/2024) (cit. on p. 64).

[64] *VCÖ-Untersuchung: Wo in österreich im Vorjahr die meisten Lkw fuhren - Mobilität mit Zukunft*, de, Mar. 2024. [Online]. Available: https://vcoe.at/presse/presseaussendungen/detail/vcoe-untersuchung-wo-in-oesterreich-im-vorjahr-die-meisten-lkw-fuhren (visited on 12/25/2024) (cit. on p. 64).

[65] *Overview - Eurostat*. [Online]. Available: https://ec.europa.eu/eurostat/web/nuts/overview (visited on 12/08/2024) (cit. on pp. 69, 70).